Mechanistic target of rapamycin (mTOR) regulates self-sustained quiescence, tumor indolence and late clinical metastasis in a Beclin-1-dependent manner.

Carole Nicco[1], Marine Thomas[1], Julie Guillermet[2], Maryline Havard[3], Fanny Laurent-Tchenio[3], Ludivine Doridot[1], François Dautry[3], Frédéric Batteux[1], Thierry Tchenio[1]*

[1] Institut Cochin, INSERM U1016/CNRS UMR 8104, Université de Paris, Paris, France.

[2] Inserm U1037, CNRS U5071, Université Toulouse III, Centre de Recherches en Cancérologie de Toulouse (CRCT), Toulouse cedex, France.[3]

[3] ENS Paris-Saclay, Université Paris-Saclay, CNRS UMR8113, IDA FR3242, Laboratory of Biology and Applied Pharmacology (LBPA), Gif-sur-Yvette, France.

E-mails: carole.nicco@inserm.fr; marine.thomas@inserm.fr; julie.guillermet@inserm.fr; mhavard@ens-paris-saclay.fr; fanny.laurent@ac-creteil.fr; ludivine.doridot@inserm.fr; fdautry@ens-paris-saclay.fr; frederic.batteux@aphp.fr

* Corresponding author

E-mail : thierry.tchenio@inserm.fr;

Abstract

Self-sustained quiescence (SSQ) has been characterized as a stable but reversible non-proliferative cellular state that limits the cloning of cultured cancer cells. By developing refined clonogenic assays, we showed here that cancer cells in SSQ can be selected with anticancer agents and that culture at low cell density induced SSQ in pancreas and prostate adenocarcinoma cells. Pre-culture of cells in 3D or their pretreatment with pharmacological inhibitors of mechanistic target of rapamycin (mTOR) synergize with low cell density for induction of SSQ in a Beclin-1-dependent manner. Dissociated pancreatic adenocarcinoma (PAAD) cells rendered defective for SSQ by down-regulating Beclin-1 expression exhibit higher tumor growth rate when injected subcutaneously into mice. Conversely, dissociated PAAD cells in SSQ promote the formation of small indolent tumors that eventually transitioned to a rapid growth phase. *Ex vivo* clonogenic assays showed that up to 40% of clonogenic cancer cells enzymatically dissociated from resected fast-growing tumors could enter SSQ, suggesting that SSQ could significantly impact the proliferation of cancer cells that are naturally dispersed from tumors. Remarkably, the kinetics of clinical metastatic recurrence in 124 patients with pancreatic adenocarcinoma included in the TGCA-PAAD project could be predicted from Beclin-1 and Cyclin-A2 mRNA levels in their primary tumor, Cyclin A2 mRNA being a marker of both cell proliferation and mTOR complex 1 activity. Overall, our data show that SSQ is likely to promote the late development of clinical metastases and suggest that identifying new agents targeting cancer cells in SSQ could help improve patient survival.

Keywords: cancer cell persistence, clonogenicity, drug resistance, prostate adenocarcinoma, pancreas adenocarcinoma, epithelial-mesenchymal transition.

Introduction

Metastases are the leading cause of cancer-related morbidity and mortality and account for more than 80% of cancer deaths. Metastasis involves cancer cells, isolated or in clusters of a few cells, that are disseminated from the primary tumors to distant sites by lymphatic or hematogenous routes. Metastases development is an inefficient process. In experimental models, only a small fraction of cancer cells that have extravasated in the parenchyma of a distant organ begins to proliferate to form micro-metastases, with most of cancer cells entering into a non-growing state called dormant [1-3]. Additionally, only a small subset of micro-metastases continue to grow to form macroscopic tumors [1-3] and the growth of small macroscopic tumors into larger tumors is also limited [4, 5]. Unfortunately, the mechanisms that limit development of metastases are also probably involved in the persistence of cancer cells in patients in complete remission and are a cause of the late development of metastases [5-7].

Since a metastase is basically a clonal cell population resulting from the proliferation of a single disseminated cancer cell, we have undertaken studies on the factors limiting the cloning of cancer cells in culture in order to better understand the factors regulating the development of metastases. This led us to discover that the ability of prostate adenocarcinoma (PA) cells to proliferate at low cell density to form a cell clone can be severely limited by a phenomenon we initially called dormancy [8, 9], by analogy with the phenomenon of cancer cell dormancy [5], then renamed Self-Sustained Quiescence (SSQ) [10] to highlight its cell-autonomous feature. Indeed, PA cells can be induced to enter a G0/G1 growth-arrested state that, once established, maintains itself at low cell density despite the return of cells to growth-permissive conditions. We showed that this self-sustained growth arrest involves a stable decrease of the redox potential of cellular thiols and is further stabilized by BMP signaling pathways [10]. Accordingly, cells in SSQ can be switched to a proliferating state when treated with SSQ inhibitors (SSQi) consisting of a reduced thiol (such as dithiothreitol, glutathione or N-

70 acetylcysteine) and/or an inhibitor of BMP signaling (such as K02288; see also the Methods
71 section for more details) [8-10]. Additionally, SSQ can be destabilized by autocrine factors of
72 less than 2 kDa produced by most types of cancer cells grown in 2D culture (see Fig S1 in [9]).
73 The self-maintenance property of SSQ is remarkable compared to other models of cancer cell
74 dormancy that in most cases involved mechanisms that are non-cell-autonomous in
75 accordance with the "seed and soil" model. This raises the issue of the biological relevance of
76 SSQ in the regulation of tumor development. Here we showed that PA and pancreatic ductal
77 adenocarcinoma (PADC) cells in SSQ or competent for SSQ can be selected with anticancer
78 agents after subculturing cells at low cell density. This allowed the characterization of factors
79 modulating induction of SSQ and the isolation of PDAC cell populations highly enriched in
80 SSQ that we used for *in vivo* studies. We then applied the results obtained to the analysis of
81 metastasis in pancreas adenocarcinoma (PAAD) patients.

82

83 # Results

84 ### *Selection of clonogenic cancer cells in SSQ with anticancer agents at low cell*
85 ### *density.*

86 We hypothesized that anticancer agents that preferentially target proliferative cells could
87 select cells in SSQ. We used KC-DT66066 cells, derived from a pancreas ductal
88 adenocarcinoma (PDAC) developed in a genetically engineered LSL-Kras$^{G12D/+}$, Pdx1-Cre
89 mouse model of spontaneous PDAC [11, 12] and routinely passaged at medium/high cell density
90 in 2D-culture plates. When these cells were plated at low cell density in regular growth
91 medium, they exhibited high cloning efficiency (CE=48 ± 14 % of seeded cells grew to form
92 cell clones; mean ± sd, n=24; see the none→ none clonogenic assay in Fig 1A-B) that was

93 slightly increased by addition of SSQi (59 ± 17 %; see the none→ SSQi clonogenic assay in
94 Fig 1A-B). To test for the selection of cancer cells in SSQ with gemcitabine, KC-DT66066
95 cells were plated at low density in regular growth medium and cultured for 3 days before
96 applying gemcitabine selection for 4 days. When cells were washed and returned to their
97 regular growth medium, very few, if any, growing cell clones were detected after 10-12 days,
98 even after microscopic examination (see gem d3→ none in Fig 1A-B). However, when cells
99 were returned to regular growth medium supplemented with SSQi after gemcitabine selection,
100 growing cell clones were recovered at an averaged frequency of 1.5% of seeded cells (see
101 gem d3→ SSQi in Fig 1A-B). This showed that non-growing cells that had survived to
102 gemcitabine treatment were in SSQ since they switched to a proliferative state only after
103 adding SSQi. Interestingly, the recovery of growing cell clones was reduced to background
104 (<0.4%) if gemcitabine was added immediately after cell seeding (see gem d0→ SSQi in Fig
105 1A-B). This indicated that most cells from 2D-cultures entered SSQ only after plating at low
106 cell density.

107 As this induction of SSQ could be counteracted by growth factors that promote cell
108 proliferation, we tested whether low fetal calf serum concentration in growth medium (low
109 FCS) could facilitate SSQ induction after plating at low cell density. After plating for 3 days
110 at low cell density in low FCS, spontaneous cloning efficiency (CE) decreased to 13% of
111 seeded cells but was increased twofold by adding SSQi (see low FCS in Fig 1A-B). This
112 suggests that clonogenic cancer cells that survive to culture at low cell density in low serum
113 were more susceptible to the stimulation of clonal cell growth by SSQi. Correspondingly,
114 frequency of cancer cells in SSQ selected by gemcitabine increased to 3.4% of seeded cells
115 under these conditions, showing that reduced serum concentration synergized with low cell
116 density to induce SSQ (see low FCS→ gem d3→ SSQi in Fig 1A-C).

117 Of note, the addition of SSQi could be delayed for at least 3 days after completion of
118 gemcitabine selection with no significant decrease of cell clone recovery, showing that SSQi
119 did not rescue cancer cells undergoing a delayed cell death phenomenon that might have been
120 induced by gemcitabine treatment (Fig S1A). In fact, the addition of SSQi at the same time as
121 gemcitabine completely blunted the subsequent recovery of growing cell clones (see low
122 FCS→ gem d3 + SSQi→ SSQi in Fig 1A-B). This showed that SSQi sensitized cells to
123 gemcitabine, as expected if the main action of SSQi is to promote the switch from SSQ to a
124 proliferative state. These observations were generalized to others pancreas and prostate cancer
125 cell lines (Fig S1B, D-E) and anticancer drugs exhibiting a strong and selective toxicity to
126 proliferating cancer cells (Fig S1D-E). Finally, we showed that SSQ entry and exit are fully
127 reversible processes that can be repeated serially since proliferating cell populations derived
128 from cancer cells in SSQ selected with nocodazole or gemcitabine and reactivated with SSQi
129 could re-enter in SSQ with high efficiency when cultured at low cell density (Fig S1F). In the
130 remainder of this article, the clonogenic assay gem d0→ SSQi was used to measure the
131 relative frequencies of cells already in SSQ in the cell populations studied (Fig 1D). The
132 relative frequency of clonogenic cancer cell in SSQ measured by clonogenic assays with
133 delayed selection by gemcitabine (gem d3→ SSQi or low FCS→ gem d3→ SSQi)
134 corresponds to the sum of the relative frequency of cancer cells already in SSQ in the cell
135 population studied and the relative frequency of their induction by low cell density and low
136 serum (Fig 1D).

137

138 ***SSQ is promoted by 3D cell culture and treatment with pharmacological***
139 ***inhibitors of mTOR.***

140 We observed that KC-A338 cells entered SSQ at high frequency in 2D culture (Fig S1B),
141 which correlated with their ability to spontaneously form transformed foci that eventually
142 detached from the bottom of the culture dish to form compact tumor spheroid-like structures
143 (Fig S1C). This led us to investigate whether 3D culture could promote SSQ. 3D culture of
144 KC-DT66066 cells on cell-surface-repellent plates in their regular growth medium resulted in
145 the formation of small, non-growing and loosely attached cell aggregates (Fig 2A-B).
146 However, when growth medium was supplemented with conditioned medium (CM) harvested
147 from senescent mouse fibroblasts cultures that produce numerous growth factors and
148 cytokines [13], compact growing spheroids were obtained (Fig 2A-B). Analysis of the
149 expression of stemness markers by RT-qPCR showed that non-growing cell aggregates
150 overexpressed *Aldh1* while growing spheroids overexpressed *Lgr5* (Fig 2C and see the S1 file
151 for the full list of genes tested). Interestingly, the gem d0 → SSQi clonogenic assay showed
152 that 6-7 % of clonogenic cancer cells had entered SSQ during 3D culture both as non-growing
153 cell aggregates or growing spheroids (Fig 2D). Moreover, cells from 3D culture exhibited an
154 increased rate of SSQ induction after plating at low density in reduced serum (compare low
155 FCS→ gem d3 → SSQi between 2D control, 3D and 3D+CM in Fig 2D). In an attempt to
156 understand why SSQ was promoted by 3D cell culture, we examined the possible role of
157 autophagy since cell detachment from the extracellular matrix can induce autophagy [14].
158 Therefore, we used the autophagy gene reporter GFP-LC3-RFP-LC3ΔG [15] to measure the
159 autophagic flux and observed that it was stably enhanced in 3D cultured cells (Fig 2E-G).
160 This led us to examine whether stimulation of autophagy in 2D cell culture could promote
161 SSQ. Accordingly, cells grown at medium cell density in standard culture plates were
162 pretreated for 1 day with Torin1 [16], a standard inhibitor of mTOR that strongly induces
163 autophagy [15], then harvested and seeded at low cell density to test for SSQ induction as
164 described in Fig 1A. Torin1 pretreatment strongly increased the induction of SSQ by plating

165 cells at low density in reduced serum (compare low FCS→ gem d3 → SSQi between
166 pretreated and non-pretreated cells in Fig 2D). Moreover, the gem d0→ SSQi clonogenic
167 assay indicated that at least 2 % of clonogenic cancer cells were induced to enter SSQ before
168 plating cells at low density. These data were confirmed using rapamycin, the canonical
169 mTOR inhibitor and both Torin1 and rapamycin also increased SSQ in human prostate
170 adenocarcinoma cell lines (Fig S2A-B). Taken together, these results showed that inhibition
171 of mTOR signaling pathways was sufficient to strongly promote the induction of SSQ in
172 cancer cells.

173

174 ***Beclin-1 expression is required for SSQ induction in an autophagy-***
175 ***independent manner.***

176 To further investigate the possible role of autophagy in regulating SSQ induction, we focused
177 on Beclin-1 (BECN1) that promotes autophagosomal membrane nucleation [17]. Beclin-1 is
178 released from the cytoskeleton upon mTOR Complex 1 (mTORC1) inhibition and is also
179 required for induction of autophagy by cell detachment from extracellular matrix [14, 18, 19]. We
180 generated 3 independent KC-DT66066 cell populations transduced with a *Becn1*-targeting
181 lentiviral shRNA that exhibited a 90% reduction in *Becn1* mRNA level, compared to cell
182 populations transduced with a *gfp*-targeting control lentiviral vector (KCsh*Becn1* and
183 KCsh*gfp* cell populations, respectively; data not shown and see below). Clonogenic assays as
184 performed in Fig 1 showed that induction of SSQ was significantly decreased by *Becn1*
185 downregulation (Fig 3A). Furthermore, this could not be alleviated by Torin1 pre-treatment of
186 cancer cells, which increased the frequencies of cells in SSQ only in control cell populations
187 (KCsh*gfp*, Fig 3B). Similar results were obtained using KC-A338 cells in which a four-fold
188 reduction in *Becn1* mRNA levels decreased SSQ induction 2.7-fold (Fig S2C).

189 Western Blot analysis showed that KCsh*Becn1* cell populations displayed a 10-fold decrease
190 of Beclin-1 (Fig 3C). Phosphorylation of p70S6 kinase and 4EBP1, two downstream targets
191 of mTOR complex 1 (mTORC1) was strongly inhibited by Torin1 treatment in both control
192 and KC*shBecn1* populations (Fig 3C). Akt1 phosphorylation at serine 473 was less affected
193 by Torin-1 treatment (Fig 3C), consistent with phosphorylation of this site by several kinases
194 in addition of mTOR complex 2 [20]. Interestingly, the expression of LC3-II (a cleavage product
195 of LC3-I (ATG8) and a marker of autophagosomes formation) showed no significant
196 difference between control and KCsh*becn1* cells under basal conditions or after treatment
197 with bafilomycin A1 (an autophagy inhibitor that induced an accumulation of LC3-II [21]; Fig
198 3C). Additionally, the level of SQSTM1, a protein degraded by autophagy, was barely
199 detectable under basal conditions in both control and KCsh*becn1* cells, but was increased by
200 bafilomycin A1 treatment (although to a lesser extent in KCsh*becn1* cells; Fig 3C). This
201 suggested that autophagy was barely affected by Beclin-1 downregulation, which was
202 confirmed by comparing autophagic flux in several independent KCsh*gfp* and KCsh*Becn1*
203 cell populations (Fig 3D). Thus, Torin1 treatment could promote SSQ through Beclin1-
204 dependent mechanisms that are unrelated to autophagy. This was confirmed by two types of
205 experiments. Inhibition of autophagic flux with bafilomycin A1 (which affects autophagy
206 downstream of Beclin-1 activation) did not have a significant impact on the induction of SSQ
207 by Torin1 in pancreas or prostate adenocarcinoma cells (Fig S2D-E). Similarly, transduction
208 of a constitutively active mutant of Beclin1, Becn1^{F121A} [22] which is defective in its binding to
209 Bcl2/Bclx inhibitors, resulted in increased autophagic flux both under basal conditions or
210 after mTOR inhibition, but did not have a significant impact on SSQ induction (Fig S2F-
211 S2H).

212

213 ***Cancer cells in SSQ are distinguished from senescent cells and exhibit***

214 ***Epithelial to Mesenchymal Transition (EMT) characteristics.***

215 Since anticancer agents are potent inducers of replicative senescence in cancer cells, we
216 investigated a possible relationship between replicative senescence and SSQ by characterizing
217 cancer cells in SSQ after gemcitabine selection. Thus, KC-DT66066 cells were treated for 1
218 day with Torin-1 at medium cell density and then individually tracked after SSQ induction at
219 low cell density using the low FCS→ gem d3→ SSQi clonogenic assay. Cancer cells in SSQ
220 were identified *post hoc* as the single cells at day 7 that survived gemcitabine selection and
221 then gave rise to a cell clone after culturing in growth medium supplemented with SSQi.
222 Accordingly, cells were photographed at the end of gemcitabine selection on day 7 (d7) and
223 after culturing in growth medium supplemented with SSQi on days 10, 14 and 17 (Fig 4A). It
224 appeared that most of the clonogenic cancer cells in SSQ were small spindle-shaped or
225 rounded cells (Fig 4B upper row and table 1). Non-clonogenic cancer cells showed more
226 variable morphology, with significantly enlarged nucleus and cell area, which are two
227 distinctive features of senescent cells [23-25] (Fig. 4B lower row and Fig 4C). In fact, a large
228 proportion of non-clonogenic cells were large, flattened senescent-like cells whereas only 1 of
229 29 clonogenic cancer cells in SSQ exhibited characteristics of senescent cells (Fig. 4B and
230 Table 1), suggesting that SSQ and replicative senescence are disjoint phenomena. This was
231 consistent with the reversible nature of SSQ (Fig S1F) whereas senescent-like cells appeared
232 to have undergone irreversible growth arrest. Indeed, two independent cell populations highly
233 enriched in cells with a senescent phenotype by culturing them for 10 days in the presence of
234 gemcitabine at medium cell density showed a strong decrease below the detection threshold in
235 their cloning efficiency and their ability to enter SSQ.

236 The spindle-shaped of most cancer cells in SSQ suggested that these cells had undergone an
237 Epithelial-Mesenchymal Transition. This was consistent with increased expression of *Snai1*, a

238 potent EMT inducer, and decreased expression of epithelial markers (*Cdh1 and Krt19*) in
239 SSQ-enriched cell populations compared to proliferating cells (Fig. 4D). Senescent cells
240 populations derived from medium cell density cultures treated with gemcitabine plus SSQi for
241 about 10 days showed no significant *Snai1* induction highlighting that *Snai1* induction in
242 SSQ-enriched cell populations did not result of their contamination by senescent cells (Fig
243 4D). The prevalence of the mesenchymal phenotype in SSQ cancer cells was supported by the
244 observation that 26 of 29 growing cell clones that formed after 3 days of culture in SSQi-
245 supplemented medium (on day 10; n= 13±7.3 cells/clone; median ± standard deviation) were
246 composed of scattered spindle-shaped cells whereas only 3 clones were epithelial type (see
247 for example Fig 4E, middle column). The persistence of a mesenchymal phenotype over
248 multiple cell generations was remarkable since native KC-DT66066 cultured at medium cell
249 density exhibited a marked epithelial phenotype (see for instance Fig S1C). However, 25 of
250 29 cell clones had switched to an epithelial phenotype by day 14 and 28 of 29 by day 17 (see
251 also Fig 4E, right column). Interestingly, a delayed transition to an epithelial phenotype was
252 significantly associated to a low clonal cell growth rate, since the 4 clones that transitioned
253 after day 14 were small compared to only 8 of the 24 that transitioned before day 14 ($p<0.02$
254 using a Fisher's exact probability test; see Fig 4E for an instance).

255

256 ***SSQ regulates tumor growth in vivo in mice.***

257 When 10^6 carefully dissociated KC-DT66066 cells harvested from growing cultures were
258 subcutaneously injected in allogenic C57Bl/6 mice, they gave rise to fast-growing tumors that
259 began to regress after approximately one week due to immune rejection of cancer cells. Even
260 during this short period of growth, we observed a higher tumor growth rate with Beclin-1
261 deficient cell population (KCsh*Becn1*) compared to the control (KCshg*fp*) (Fig S3A).
262 Interestingly, we found that treatment with a high dose of gemcitabine on day 4 after cell

263 injection increased KC cell tumorigenicity, possibly by depressing the immune response (data
264 not shown and see [26]). Under these conditions, the higher growth rate of KCsh*Becn1* cells was
265 confirmed because KCsh*becn1* cells, but not the control population, were able to out-compete
266 the immune response (Fig S3B). Considering that KCsh*becn1* and KCshg*fp* cell populations
267 exhibited the same growth rate in 2D culture at medium cell density (Fig S3C) and the same
268 percentage of clonogenic cells (compare none→ SSQi in Figs 3A and 3B), these experiments
269 suggested that a significant fraction of control cells could enter SSQ *in vivo*, resulting in a
270 lower tumor growth rate. Of note, they also showed that KC-DT66066 cells exhibit high
271 resistance to gemcitabine *in vivo*, which is not dependent on Beclin-1 expression. To further
272 investigate the role of SSQ in regulating tumor growth, we analyzed the tumorigenicity of
273 KC-DT66066 cells in immunodeficient NOD-SCID mice. As few as 100 dissociated cells
274 harvested from exponentially growing cell cultures gave rise to rapidly growing tumors in
275 these hosts (Fig S3D). To test the contribution of cells in SSQ, we subcutaneously injected 4
276 mice with 500 cells obtained from exponentially-growing culture (which were refer to as the
277 Exp group that additionally included 2 mice previously injected with 100 proliferating cells,
278 n=6) and 8 mice with 500 cells enriched for SSQ by Torin 1 treatment and gemcitabine
279 selection in cell culture (Fig 5A and Methods). Mice injected with cells enriched for SSQ
280 were further divided into 2 groups that were treated with saline (Ssq/none group, n=4) and
281 gemcitabine on the 4th and 11th day after cell injection (Ssq/gem group, n=4; Fig 5A and
282 Methods). Gemcitabine treatment was performed with the aim of counter selecting cancer
283 cells that started to proliferate shortly after cell injection to further enrich the injected cells for
284 SSQ cells *in vivo*. A distinct palpable tumor mass (≈10 mm^3) could be detected in all the mice
285 in the Exp and Ssq/none groups and in 3 of the 4 mice in the Ssq/gem group around the 30th
286 day after cell injection (Fig 5B-C). These results indicated that the initial phase of tumor
287 growth was not significantly affected by the state of the cells prior to injection or by treatment

288 with gemcitabine. However, subsequent tumor growth differed in the groups of mice injected
289 with SSQ cells. While all tumors in mice of the Exp group grew vigorously and rapidly
290 reached a tumor volume of 100 mm^3 approximately one week later (36.7 ± 3.9 days, mean ±
291 s.d., n=6), 2 tumors out of 4 in mice in the SSQ/none group thereafter grew very slowly and
292 reached 100 mm^3 only at day 67 after cell injection. This corresponded to a difference with
293 the mean tumor growth time of the Exp group of more than 7 times the standard deviation of
294 the tumor growth times in the Exp group (Fig 5B and 5D). Such a difference makes the
295 occurrence of slow-growing tumors unlikely in the Exp group if a Gaussian distribution of
296 tumor growth rates in this group is assumed. Additionally, a third mouse in the Ssq/none
297 group developed a tumor that rapidly reached 200 mm^3 on day 37, but then stopped growing
298 until this mouse was sacrificed on day 47 due to skin ulceration (Fig 5B). The proportions of
299 slow-growing tumors in the Exp and Ssq/none groups (0/6 *vs* 3/4) were found statistically
300 different as calculated with a Fisher's exact probability test (p=0.033). This confirmed that
301 formation of tumors with a slow-growing phenotype is promoted by the injection of cancer
302 cells in SSQ. Similar observations were made with mice in the Ssq/gem group (3 of 4 mice
303 also developed slow-growing tumors), but one mouse also showed delayed formation of a
304 palpable tumor (it was detected on day 65 after cell inoculation; Fig 5B) in addition to slow
305 tumor growth (Fig 5D). This showed that cancer cells in SSQ promoted the formation of
306 indolent tumors at high frequency and that SSQ could also impede the early phase of tumor
307 growth. Nonetheless, all of the indolent tumors, including the one that had been indolent for
308 two months, eventually transitioned to a rapidly growing phase, consistent with our concept
309 of a stable but reversible quiescence (Fig 5B). Genes expression profiling of growing tumors
310 by RT-qPCR analysis did not reveal any significant difference associated with the status of
311 the injected cells (correlation coefficient r>0.99, n = 17 genes analyzed, p <0.0001; Fig S3E
312 and S1 file). Interestingly, in comparison with exponentially growing KC-DT66066 cells in

313 2D-cultures, all growing tumors displayed an increased expression level of the *Lgr5* stemness
314 marker, as observed for cells growing in spheroids (compare Figs 2C and S3E). This analogy
315 between spheroids and tumors was further supported by analysis of the clonogenicity of
316 dissociated tumor cells, as previously done for spheroids (Fig 2D, 5E and see Methods). This
317 not only confirmed the presence within the tumors of significant populations of cells in SSQ
318 (18.7± 8.2% of clonogenic tumor cells selected with the gem d0 clonogenic assay, mean ± sd,
319 n=5; Fig 5E), but also revealed that clonogenic tumor cells were prone to enter SSQ (27.3 ±
320 11.4% of clonogenic tumor cells selected with the low FCS→ gem d3→ SSQi clonogenic
321 assay, mean ± sd; n=5; Fig 5E). Interestingly, in tumors that grew in allogenic C57Bl/6 mice
322 injected with 10^6 proliferating KC-DT66066 cells, clonogenic assays also revealed cancer
323 cells in SSQ or prone to enter SSQ after seeding at low cell density under low serum, but at
324 lower frequencies (1.3 ± 0.7% and 3.0 ± 1.7% of clonogenic cells, respectively, mean ± sd,
325 n=5). However, these frequencies significantly increased when C57Bl/6 mice were treated
326 with cyclosporine, an immunosuppressive agent (4.50±1.1% and 14.8±4.9% of clonogenic
327 cells, respectively; n=4, $p<0.002$; see Methods for more details), suggesting that immune
328 response could modulate frequency of SSQ cells in tumors.

329

330 ***High Beclin-1 level and low mTOR activity in the primary tumor of PAAD***
331 ***patients is predictive of late metastatic recurrence.***

332 Based on our results in mice, primary tumors with a relatively low level of Beclin-1
333 expression should release cancer cells that are not prone to enter SSQ, and thus cause a lower
334 rate of late metastasis if SSQ constitutes the only mechanism controlling delayed metastases
335 development in pancreatic adenocarcinoma (PAAD). Analysis of PAAD patient records
336 downloaded from the Genomic Data Commons website (see Methods) showed that the rate of

337 distant metastases in the first 360 days after initial treatment did not differ significantly
338 between cohorts of patients with low and high level of Beclin-1 transcripts in their primary
339 tumors (Fig 6A). However, beyond 360 days, a low level of Beclin-1 transcripts in the
340 primary tumor was associated with a decreased rate of distant metastases (Fig 6B and see the
341 Methods section for the determination of the cutoff value of *BECN1* mRNA levels used
342 throughout this study**)**. This remained true when we restricted the analysis to patients with a
343 similar T3N1M0/Mx clinical grade (Fig S4A-B), suggesting that Beclin-1 expression level is
344 a predictive factor of late metastasis independent of TNM grade. To further establish the
345 biological relevance of a 360-day cutoff for classifying patients as developing early or late
346 metastases, we compared the primary tumors transcriptomes of patients with distant
347 metastasis-free survival less than and greater than 360 days by Gene Set Enrichment Analysis
348 (GSEA). GSEA recovered only 8 statistically significant genes sets with a false discovery rate
349 (FDR) $q<0.05$. They showed that primary tumors from patients with a distant-metastasis-free
350 survival inferior to 360 days were enriched for genes regulated by MYC transcription factor,
351 mTORC1 signaling and the unfolded protein response (Fig 6C and see Fig S4C for others
352 miscellaneous gene sets). This suggested that a distinguishing feature of tumors from patients
353 with a distant metastasis-free survival inferior to 360 days might be enrichment in
354 proliferating cells (enhanced MYC activity) that exhibited higher protein synthesis (enhanced
355 mTORC1 signaling) associated with endoreticulum stress (enhanced unfolded protein
356 response). Thus, we analyzed distant metastasis-free survival of PAAD patients according to
357 the relative level of Cyclin A2 (*CCNA2*, a marker of cell proliferation) in their primary tumor
358 since mTORC1 activity seemed to be associated to tumor cell proliferation in the primary
359 tumors. A high level of Cyclin A2 transcript was found to be a very strong predictor of early
360 metastasis with a median survival time of 291 days *versus* 763 days in the cohort of patients
361 with a low level of Cyclin A2 transcript (Fig 7A and see the Methods section for the

362 determination of the cutoff value of CCNA2 mRNA levels used throughout this study) and
363 this was independent of TNM grade (Fig S4D). Independence was also confirmed by
364 multivariate Cox regression analysis (data not shown). GSEA showed that primary tumors
365 with a high level of Cyclin A2 transcripts were highly enriched for classical hallmarks of cell
366 proliferation, but also enhanced mTORC1 signaling and unfolded protein response (Fig 7B
367 and S4E), as anticipated above. The strong correlation between the transcript levels of Cyclin
368 A2 and of markers of mTORC1 activity in the primary tumors of PAAD patients were
369 confirmed by hierarchical gene clustering (Fig 7C). Interestingly, this analysis also showed
370 that levels of Beclin-1 and Cyclin A2 transcripts (as well as mTORC1 activity marker genes)
371 were positively correlated with levels of cancer cell markers but not mesenchymal,
372 endothelial or immune cell markers (Figs 6C and S4F). This suggested that transcript levels of
373 Beclin-1 and Cyclin A2 in the primary tumors were mainly determined by cancer cells.

374 The combination of Beclin-1 and Cyclin A2 markers showed that all metastatic events within
375 the first 360 days after initial treatment were associated with tumors with either high Cyclin
376 A2 or both low Cyclin A2 and low Beclin-1 expression (Fig 7D). Remarkably, patients whose
377 tumors exhibited both low Cyclin A2 and high Beclin-1 expression did not develop
378 metastases within the first 360 days after initial treatment (Fig 7D). However, after 360 days,
379 patients with both low Cyclin A2 and high Beclin-1 expression exhibited a higher rate of
380 distant metastasis compared to patients with both low Cyclin A2 and low Beclin-1 expression
381 in their primary tumors (Fig 7E). Taken together, this strongly suggests that Beclin-1
382 abundance and mTORC1 activity in the primary tumor of PAAD patients determine the
383 kinetics of occurrence of clinical metastases. This was further confirmed by analyzing the
384 statistics of the relative proportions of early and late clinical metastasis (before and after 360
385 days) according to tumor phenotype of patients with a T3N1M0/x clinical grade (Table 2).
386 This showed that late clinical metastasis was mainly associated to the $CCNA2^{low}$ $BECN1^{high}$

387 primary tumor phenotype and early clinical metastasis to the *CCNA2*^{high} and the *CCNA2l*^{ow}
388 *BECN1*^{low} primary tumor phenotypes.

389

390 Discussion

391 We showed here that cancer cells in SSQ can be selected with anticancer agents including
392 gemcitabine, vincristine, nocodazole, doxorubicin, oxaliplatin and taxol *in vitro* (Figs 1, S1D-
393 F) and possibly also *in vivo* (Fig 5A-B). This suggests that SSQ could promote the persistence
394 of disseminated cancer cells after adjuvant chemotherapies. Analysis of the mechanisms of
395 SSQ induction showed that culture at low cell density induces SSQ in prostatic and pancreatic
396 adenocarcinoma cells (Fig 1B and [9, 10]). By investigating why SSQ is also induced at high cell
397 density in non-growing cell aggregates or in growing cancer cell spheroids generated in 3D
398 culture (Fig 2D), we found that it is induced by mTOR inhibition. Indeed, pretreatment of
399 growing cancer cells cultured in 2D at medium cell density with rapamycin or Torin1, two
400 standard pharmacological inhibitors of mTOR activity, is sufficient to induce SSQ and also
401 synergizes with low cell density for SSQ induction (Figs 2H and S2A-B). As cell proliferation
402 depends on mTOR activity [27-29], this implies that proliferating cells are not prone to enter
403 SSQ, in agreement with our finding that exponentially growing cell cultures in 2D exhibited
404 low frequency of cancer cells already in SSQ and are modestly induced to enter SSQ after
405 seeding at low cell density (Fig 1B). Inversely, in 3D cultures, high levels of autophagy
406 indicate that mTOR activity was downregulated in a large fraction of cells since mTOR
407 activity inhibits autophagy. An unexpected result is that induction of SSQ requires Beclin-1
408 expression but was independent from autophagy. Indeed, downregulation of Beclin-1 inhibits
409 SSQ induction but not of autophagy (Fig 3) and autophagy inhibition with bafilomycin A1
410 does not prevent SSQ induction by Torin1 (Fig S2D-E). Moreover, transduction of a

411 constitutively active Beclin-1 mutant, defective in its binding to Bcl2/Bclx inhibitors,
412 increased both basal autophagy flux and its stimulation by mTOR inhibitors, but had no effect
413 on SSQ induction (Fig S2F-H). This confirmed that autophagic flux does not regulates SSQ
414 induction and thus that Beclin-1 is likely to be required for SSQ through autophagy-
415 independent pathways. Several publications have already reported autophagy-independent
416 roles for Beclin-1. Beclin-1 regulates degradation of cell membrane receptors for growth
417 factors and transferrin through the control of endolysosomal trafficking [17, 30-32]. It can also
418 inhibit the System Xc^- cystine/glutamate antiporter involved in cystine uptake, thus impacting
419 cellular thiol redox potential [33], and also the Stat3 signaling pathway [34]. These actions of
420 Beclin-1 could contribute to two main features of cancer cells in SSQ which are the absence
421 of proliferating response to stimulation by external growth factors and a decrease in the redox
422 potential of cellular thiols. Considering that mTOR activity is regulated by nutrient depletion,
423 cellular thiol redox potential and growth factor signaling [35-45], activation of Beclin-1 through
424 inhibition of mTOR activity could therefore promote the establishment of a self-sustained
425 inhibitory loop maintaining a low mTOR activity (Fig 8). As mTOR also directly control cell
426 proliferation through its regulation of c-Myc activity and Cyclin D accumulation [27-29], our
427 data point towards a central role of mTOR downregulation in the induction and maintenance
428 of self-sustained quiescence (Fig 8). An issue of this study concerns the role of EMT in SSQ.
429 We observed that pancreas cancer cells in SSQ exhibit a mesenchymal phenotype (Fig 4B, D
430 and E). This mesenchymal phenotype is obviously not sufficient to maintain SSQ since it
431 often persisted for several cell generations after the transition from SSQ to a proliferating
432 state. However, it could promote the transition between proliferating and SSQ states. This
433 would be consistent with the high frequency of the mesenchymal phenotype in SSQ cancer
434 cells. Additionally, the slower growth of cell clones with a mesenchymal phenotype could

435 also result from a higher rate of mesenchymal cell reentry in SSQ (see Fig 4E and the
436 corresponding Results section).

437 Another result of our work is that dissociated PADC cells in SSQ injected into mice promoted
438 the delayed formation of a palpable tumor in one case, as expected for the dormant phenotype
439 of cancer cells in SSQ *in vitro*, but also, quite unexpectedly, the formation of small, slow-
440 growing (indolent) tumors in most cases (Fig 5). Our data suggest that SSQ can directly
441 regulate tumor cell growth and thus tumor indolence when tumor is composed of a high
442 percentage of SSQ-competent cells. Indeed, we observed that the mouse tumor
443 microenvironment promotes SSQ. A large fraction of clonogenic cancer cells dissociated
444 from resected tumors were found to be in SSQ or prone to enter SSQ after cell plating at low
445 cell density, this even in tumors resulting from the injection of exponentially growing cancer
446 cells exhibiting a low frequency of cells in SSQ or competent for SSQ (see the Result section
447 and also compare data in Figs 1 and 5E). This SSQ-promoting effect of tumor
448 microenvironment could explain why tumors generated by the injection of a large number of
449 exponentially growing cancer cells rapidly exhibit a higher growth rate when these cells have
450 been made defective for SSQ by Beclin-1 downregulation whereas downregulation of Beclin-
451 1 has no effect on proliferation of cells cultured at medium cell density (Fig S3A-C).
452 Accordingly, a plausible mechanism of long-term tumor indolence is the maintenance of a
453 high percentage of cancer cells in SSQ through the continuous induction of SSQ by tumor
454 microenvironment (see also above the discussion on the possible role of EMT in SSQ
455 reentry). Breaking this steady state through the rapid outgrowth of cancer cells refractory to
456 SSQ induction or changes in the tumor microenvironment would resume a high tumor growth
457 rate. Taken together, these results challenges models of tumor dormancy that posit a dynamic
458 balance between cancer cell proliferation and cell death caused by antitumor immunity and
459 insufficient tumor vascularization [46].

460 Our analysis of the relationship between metastasis in PAAD patients and gene expression in
461 their primary tumor showed that tumors that are expected to contain and therefore disseminate
462 clonogenic cancer cells that are not prone to enter SSQ mainly give rise to early clinical
463 metastasis whereas those that are likely to disseminate cancer cells in SSQ or poised to enter
464 SSQ give rise to late clinical metastasis (Figs 5-6 and Table 2). Indeed, tumors expressing a
465 higher level of Cyclin A2, a marker of cell proliferation, also exhibit higher mTORC1 activity
466 (Fig 7B-C), which inhibits induction of SSQ (see discussion above and Fig 8). Similarly, a
467 low level of Beclin-1 transcripts was found to decrease the ability to enter SSQ (Fig 3), even
468 in growth-arrested cells cultured in 3D (data not shown). Conversely, a high level of Beclin-1
469 expression, when combined with low mTORC1 activity associated with low Cyclin A2
470 expression, is expected to promote entry in SSQ (Fig 3). Of note, Cyclin A2 mRNA, in
471 addition to being a marker of cell proliferation, is also a hallmark of c-Myc activity (it is the
472 highest ranked gene in the GSEA analyses showing enrichment for c-Myc targets in Fig 7B
473 and the eighteenth ranked gene in Fig 6C). Correlatively, one of the most distinctive features
474 of patients with early metastasis is an enrichment of their primary tumor with cellular markers
475 of c-Myc activity (Figs 6C and 7B). This suggests that c-Myc activity *per se* could be a better
476 hallmark of mTORC1 activity in primary tumors rather than cell proliferation, which is
477 consistent with c-Myc regulation by mTORC1 signaling via Beclin-1-dependent and
478 independent pathways [27, 47].

479 Beclin-1 is often considered a haplo-insufficient tumor suppressor gene since Beclin-1 can
480 inhibit tumorigenesis [48] and an allele of this gene is frequently deleted in advanced cancers [49].
481 A high Beclin-1 expression level in the primary tumor of PAAD patients was successively
482 associated with a low rate of metastasis in one study and then with a high rate of metastasis in
483 another [50, 51]. This paradox could partly result from the short follow-up of patients with high
484 Beclin-1 in the first study, since we found that high Beclin-1 expression shows a trend to

485 promote a lower rate of early metastasis (Fig 6A). However, it should be noted that our data
486 support the idea that Beclin-1, combined with mTORC1 activity, primarily determines the
487 kinetics of metastases development and not the overall rate of metastasis.

488 A possible direct clinical application of our results is a better selection of patients eligible for
489 early and aggressive adjuvant chemotherapy. Indeed, our results suggest that patients with a
490 primary tumor associated to dispersion of cancer cells not entering SSQ could benefit from
491 aggressive chemotherapy since their dispersed cancer cells are expected to be sensitive to
492 anticancer agents. It is crucial that adjuvant chemotherapy begins as early as possible since
493 cancer cells grown in tumor masses gained new mechanisms of resistance to anticancer agents
494 compared to dispersed cancer cells, including the possible *de novo* generation of cancer cells
495 in SSQ within growing metastases microenvironment. Patients with dispersed cancer cells
496 only in SSQ (patients with a primary tumor phenotype associated to late metastasis or treated
497 once by an aggressive adjuvant chemotherapy) are unlikely to respond well to chemotherapy
498 since these cancer cells are resistant to anticancer agents even when they are dispersed.
499 Therefore, the development of new agents targeting cancer cells in SSQ seems essential.
500 Complete elimination of dispersed cancer cells in SSQ may require the identification of
501 agents that are effective in stably reversing SSQ *in vivo* to restore cancer cell susceptibility to
502 chemotherapy or in directly killing cancer cells in SSQ.

503

504 # Materials and Methods

505 **Cells:** All cells were cultured under 5% CO_2 at 37 °C in Dulbecco's Modified Eagle's
506 Medium-high glucose (4.5 $g.L^{-1}$ glucose, glutamax 1X; #D0819 Sigma Aldrich)
507 supplemented with fetal calf serum (10% of DMEM volume; #10270-106; various lots;
508 GIBCO, Life Technologies), pyruvate 1 mM (#CSTVAT00-0U from EUROBIO),

509 penicillin/streptomycin 1X (#15140-122 from GIBCO), to which distilled water was added
510 (17.6% of DMEM volume) to make it isotonic (isoDMEM-FCS). Final fetal calf serum (FCS)
511 concentration was 7.9% in growth medium and was decreased to 1.9% for low FCS condition
512 by dilution with growth medium without FCS. For subculturing, cells were harvested after 5
513 min treatment with 0.25% trypsin-EDTA (#25200-056 from Gibco) supplemented with 1 mM
514 pyruvate (Tryp-EDTA-Pyr), dissociated by pipetting, counted using a hemocytometer if
515 necessary and inoculated at a dilute density. KC-DT66066, KC-A338, and KPC-A219 are
516 independent cell lines derived from pancreas ductal adenocarcinoma (PDAC) developed in
517 genetically engineered LSL-*Kras*$^{G12D/+}$, Pdx1-*Cre* (KC) and LSL-*Trp53*$^{R172H/+}$, LSL-
518 *Kras*$^{G12D/+}$, Pdx1-Cre (KPC) mouse models of spontaneous PDAC, respectively [11, 12]. All KC
519 and KPC-A219 cells were derived in J. Guillermet laboratory under a genetic C57Bl/6 x CD1
520 and C57Bl/6 x CD1 x 129 genetic background, respectively, and were authenticated by PCR.
521 Human LNCaP* and LNCaP C4-2 (RRID:CVCL_4782) prostate adenocarcinoma were
522 characterized previously [10]. Cells were found to be free of mycoplasma by a PCR test carried
523 out on their supernatant.

524

525 **Reagents:** anti-Beclin-1 (clone D40C5, #3495S), anti-GAPDH (clone D16H11, #5174), anti-
526 4E-BP1 (clone53H11, #9644), anti-phospho-4E-BP1 (Thr37/46; clone236B4, #2855), anti
527 p70 S6 kinase (clone 49D7, #2708), anti-phospho-p70 S6 kinase (Thr389) (clone 108D2,
528 #9234) and anti-LC3A/B (clone D3U4C, #12741) were rabbit monoclonal antibodies from
529 Cell Signaling Technology. Anti-Akt (#9272) and anti-phospho-Akt (S473; #9271) were
530 rabbit polyclonal antibodies from Cell Signaling Technology. Anti-SQSTM1 (#GT239) was a
531 mouse monoclonal antibody from Invitrogen. Secondary HRP-linked anti mouse IgG
532 (7#076S) and anti rabbit IgG (#7074S) were from Cell Signaling Technology. K02288 (#AB-
533 M2789-10MG), Torin1 (#F6100-UBP) and rapamycin (#AB-M1768-25MG) from AbMole

534 BioScience (USA), N-acetyl-L-cysteine (#A7250) from Sigma-Aldrich, Nocodazole (#F6120-
535 UBP) was from UPBIO. Gemcitabine chlorhydrate and Cyclosporin A were from Sandoz
536 (France) and Vincristine Sulfate from Hospira (France). Lipofectamine 3000 kit (#L3000-00)
537 was from Invitrogen. LightCycler 480 SYBR Green I Master kit (#04707516001) was from
538 Roche Diagnostics, USA)

539

540 **Clonogenic assays**: 2D-cultured murine pancreas and human prostate C4-2 cells were seeded
541 at 10^3 cells per 60 mm diameter tissue culture-treated polystyrene dish (#430169, Corning,
542 NY, USA) for selection of SSQ cells with anticancer agents, otherwise at 10^2 cells per dish
543 and cultured as indicated. Human LNCaP* cells were seeded at 5000 cells per 6 cm diameter
544 dish and cultured as indicated. To test the cloning efficiency (CE) of cells from 3D-cultures,
545 cells were harvested, washed one time with Tryp-EDTA-Pyr and then dissociated by
546 incubation for 20 minutes in Tryp-EDTA-Pyr at 37°C with regular pipetting. Complete
547 growth medium was added and cells were filtered through a 70µm Cell Strainer (Falcon,
548 Corning), washed once with complete growth medium, counted and plated at low cell density
549 as needed. For the CE tumor cell assay, tumors were minced and cells dissociated using the
550 same protocol as for spheroids. Only cells larger than 20 µm were counted with a
551 hemocytometer to calculate cell dilutions for clonogenic assays (cells smaller than 20 µM
552 were not clonogenic). In 7 of the 8 tumors analyzed, more than 90% of the clonogenic tumor
553 cells were KC-DT66066 cells that generated easily recognizable dense and rapidly growing
554 cell clones. In 1 tumor from the Ssq/none group that was not included in CE analysis, long-
555 lived fibroblastic cells constituted more than 90% of the clonogenic tumor cells and generated
556 only sparse, slow-growing fibroblastic cell clones. Cell clones were fixed in 50% ethanol and
557 10% acetic acid, stained with Crystal Violet and counted manually (clones with a diameter >
558 0.5 mm). Cloning efficiency (CE) was calculated as the ratio of the number of cell clones to

559 that of seeded cells. Cloning efficiency in the presence of SSQ inhibitors (SSQi) was used as
560 a measure of the percentage of clonogenic cells. The fraction of cells in SSQ in a cell
561 population was defined as the cloning efficiency of cells from that population in the gem d0→
562 SSQi clonogenic assay (Fig 1A and main text). SSQi (NK, GK or GSK) consisted of a
563 reduced thiol (N-Acetylcysteine (NAC or N) or glutathione (G) which could be used with
564 similar efficacy at optimal concentrations) at 1 or 4 mM for murine and human cells,
565 respectively, and of K02288 (K, an inhibitor of BMP signaling) at 100 nM. In murine PDAC
566 cells, K02288 increased by about twofold the recovery of proliferating cell clones from cells
567 in SSQ when NAC concentration was below 0.5 mM but was otherwise unnecessary at 1 mM
568 NAC concentration. Similarly, SB505124 (an inhibitor of TGF□ signaling) was used with
569 K002288 and glutathione (GSK) to reverse SSQ in LNCaP* cells, but its effect was
570 statistically insignificant.

571

572 **3D culture:** Cells were harvested from 2D cultures by treatment with Tryp-EDTA-Pyr,
573 counted and seeded into 24 well-plates (Cellstar, cell-repellent surface, #664970, Greiner Bio-
574 One Gmbh) or into 6 cm dishes (Ultra-Low Attachment, #3261, Corning, NY, USA) at a
575 concentration of 10^4 and 10^5 cells per well or dish, respectively, in regular growth medium
576 and cultured for up to 11 days. Conditioned Medium (CM) was isoDMEM-FCS harvested
577 from primary cultures of fibroblasts derived from 13.5 days C57Bl/6 embryos and made
578 senescent by gemcitabine treatment at 100 ng/ml for 7 days. The CM was filtered through 0.2
579 µm sized-pore filter and in some experiments concentrated with Amicon Ultra centrifugal
580 filters with a cut-off of 50 kDa or 300 kDa.

581

582 **Identification of cancer cells in SSQ in low density 2D KC-DT66066 cell culture:**
583 Individual cancer cells pretreated with Torin-1 at medium cell density were followed from
584 day 7 of the low FCS→ gem d3→ SSQi clonogenic assay by photographing them with a
585 Olympus IX70 inverted phase contrast microscope using 20X LCPlan FI Ph1 and 10X UPlan
586 F1 Ph1 objectives and a mounted Canon EOS 6D camera. Pictures (in jpg format ; 5 to 12
587 pixels per microns) were manually analyzed using the polygonal enclosing tool of ImageJ. In
588 spindle-shaped cells, the nuclear membrane was often indistinct, so we measured area of a
589 nuclear region including nucleus and/or a perinuclear region enriched in vesicles, both
590 exhibiting a specific granular texture and dark yellow-brown color (see Fig 4B). The mean
591 value of the area of this nuclear region was close to that of the area of the nucleus measured in
592 confluent KC-DT66066 cells in which nuclear membrane was unambiguously identified.

593

594 **Recombinant retrovirus:** To downregulate *Beclin-1* expression we used recombinant
595 lentiviral vectors, pLKO1-sh*Becn1*, that encode validated shRNA [52, 53] from the RNAi
596 Consortium (clones TRCN0000087290 and TRCN0000087292 with target sequence 5'-
597 GCGGGAGTATAGTGAGTTTAA-3' and 5'-CGGACAGTTTGGCACAATCAA-3',
598 respectively, distributed by Sigma-Aldrich, Merck, France. pLKO1-sh*gfp* [54] was a gift from
599 David Sabatini (Addgene plasmid # 30323 ; http://n2t.net/addgene:30323 ;
600 RRID:Addgene_30323), pMRX-IP-GFP-LC3-RFP-LC3ΔG [15] a gift from Noboru Mizushima
601 (Addgene plasmid # 84572 ; http://n2t.net/addgene:84572 ; RRID:Addgene_84572) and lenti-
602 HA-mBec1 F121A [22] a gift from Congcong He (Addgene plasmid # 99506 ;
603 http://n2t.net/addgene:99506 ; RRID:Addgene_99506). To produce retroviral particles, 2 µg
604 of the plasmid carrying the relevant recombinant provirus was co-transfected with 2 µg of
605 plasmid pMD2.G (a kind gift from D. Trono) and 2 µg of plasmid PVPackgagpol (#217566
606 from Stratagene, La Jolla, CA) or plasmid pCMV-ΔR8.74 (a gift from D. Trono) (for

607 Moloney Murine Leukemia Virus and Human Immunodeficiency Virus derived retroviral
608 backbone, respectively) in 90% confluent HEK293T cells plated in 6 cm diameter dishes
609 using lipofectamine 3000 kit (12 µL of P3000 and 14 µL of Lipofectamine 3000 used).
610 Supernatant were filtered through 0.4 µM filter and used to infect exponentially growing
611 cells. Transduced cells were selected with puromycin (Calbiochem; 1 to 2 µg/ml) or directly
612 used in some superinfection experiments with pMRX-IP-GFP-LC3-RFP-LC3ΔG.

613

614 **Flow cytometry analysis of autophagic flux:** Cell transduced with MRX-IP-GFP-LC3-RFP-
615 LC3ΔG vector were seeded at 4 x 10^5 cells per 6 cm diameter dish (day 0), treated at day 1 as
616 indicated and dissociated and harvested in cold culture medium at day 2 by strong pipetting
617 after Tryp-EDTA-Pyr treatment, pelleted by centrifugation, resuspended in 500 µL of cold
618 PBS 1X and fixed by adding 4.5 mL of 4 % paraformaldehyde in saline (sc-281692, Santa
619 Cruz Biotechnology, France) and incubating at room temperature for 5 minutes. Then, cells
620 were washed 2 times with PBS1X, suspended in 500 µL PBS 1X and kept at 4°C in dark until
621 analysis. The GFP and RFP cell fluorescence was measured using a Fortessa Flow-cytometer
622 (BD Biosciences) with excitation/emission at 488/515-545 and 561/600-620 nm respectively.
623 For data analysis using FlowJo software (BD Biosciences), the RFP positive cell
624 subpopulation was first selected to measure the GFP/RFP fluorescence ratio. The prior
625 elimination of cell doublets did not have a significant impact on the results.

626

627 **mRNA isolation and RT-qPCR analysis:** Cultured cells or spheroids were washed twice
628 with cold PBS, and processed for total RNA isolation using the RNeasy Mini Kit (Qiagen,
629 France) or Trizol reagent (Invitrogen, ThermoFisher Scientific, France). Tumor fragments
630 were minced into fine pieces and lysed by vigorous shaking with steel balls in Trizol reagent.

631 RT-qPCR experiments were performed as previously published [8, 10] using the LightCycler 480
632 SYBR Green I Master kit. *Hprt* was selected as the reference gene for normalization of data
633 derived from independent cDNA synthesis reactions and normalization was further checked
634 using others control gene such as *Sdha* or *Rplp0*. The expression level of each mRNA species
635 was further normalized to that measured in the growing 2D-culture (KC-2D) set to 1.
636 Oligonucleotide primers sequences along with a summary of data are shown in **S1 file**.

637

638 **Western blot analysis:** Cells were seeded at 4 x 10^5 cells per 6 cm diameter dish (day 0),
639 treated at day 1 as indicated and lysed at day 2 or 3. For cell lysis, cells were washed two
640 times with cold PBS1X and lysed in Laemli 2X lysis buffer supplemented with phosphatase
641 inhibitors. About 50 µg protein lysate were subjected to SDS-PAGE and transferred to a
642 polyvinylidene fluoride membrane (Hybond P; RPN303F from Amersham Pharmacia
643 Biotech, England) that was blocked with 5% non-fat milk, in PBS1X containing 0.1% Tween-
644 20 and probed with primary antibodies in the same buffer overnight at 4°C. Proteins were
645 detected using horseradish peroxidase-conjugated secondary antibodies and detected using
646 ECL (RPN2106) or ECL-select (RPN2235) reagents (Amersham, GE Healthcare, UK) and a
647 cooled digital camera (LC33000, FujiFilm). Relative protein levels in each lane was measured
648 using the Multi Gauge software (Fuji Microsoft, FujiFilm) associated to the digital camera
649 device.

650

651 **Animal models:** Six-week-old female *NOD.CB-17-Prkdc scid/Rj* (NOD-SCID) or C57Bl/6 J
652 mice weighing 16–20 g were purchased from Janvier Laboratory (Le Genest Saint Isle,
653 France). All mice were housed in ventilated cages with sterile food and water *ad libitum*
654 throughout the study. The presence of subcutaneous tumors was carefully checked by

655 palpation, light pinching and rolling of the skin between fingers to assess thickening of the
656 skin and the presence of small hard lumps, which allowed to detect most of the tumors several
657 days before they reach 1 mm^3. Tumor size was measured two times a week with Vernier
658 calipers. Tumor volumes were calculated using the following formula: $(L * W^2)/2$, in which L
659 represents the large diameter of the tumor, and W represents the small diameter. Mice were
660 sacrificed when their tumor volume exceeded 1500 mm^3 or when they showed signs of
661 suffering.

662

663 **Experimental procedures for NOD-SCID mice:** KC-DT66066 cells in SSQ were generated
664 in two steps. 4 x 10^5 cells were seeded in 6 cm diameter dish and treated the next day with
665 200 nM Torin1 for 1 day. Cells were then subcultured at low cell density in growth medium
666 with 1.9% FCS plus insulin 10 μg/mL (to enhance survival of cells in SSQ) for 3 days and
667 then subjected to gemcitabine selection for 5 days in regular medium supplemented with
668 gemcitabine at 30 ng/mL. Cells in SSQ were then harvested in DMEM with 10% fetal calf
669 serum after 5 min treatment with Tryp-EDTA-Pyr solution warmed to 37°C, washed two
670 times with cold DMEM without serum or antibiotics, resuspended in a small volume of
671 DMEM and counted. Exponentially growing cells were harvested from 6 cm diameter dishes
672 seeded with 4 x 10^5 cells two days before and harvested as cells in SSQ in DMEM. Harvested
673 cells were injected subcutaneously in the backs of mice. Gemcitabine at 50 mg/kg was
674 injected intraperitoneally on day 4 and 11 for the Ssq/gem group, day 0 referring to the day of
675 cell injection.

676

677 **Experimental procedures for C57Bl/6 mice.** Cells were seeded at 4 x 10^5 per 10 cm
678 diameter plate and then cultured for 4 or 5 days with a growth medium change on the third

679 day. Cells were harvested by a 3 min treatment with Tryp-EDTA-Pyr, washed twice with
680 growth medium without serum or antibiotics, filtered through a 70 µm cell strainer and 200 µl
681 of a cell suspension at 5 x 10^6 cells/mL subcutaneously injected (day 0) into the back of
682 C57Bl/6 mice. Cyclosporin A (Sandoz, France) was administered orally at a dose of 80 mg/kg
683 at days -2, 0, 4, 7 and 11.

684

685 **Analysis of patients' records**: The anonymized records from 144 patients with pancreatic
686 adenocarcinoma (PAAD) included in the TGCA-PAAD project and with a follow up and a
687 transcriptome profiling of their primary tumors by Illumina sequencing were downloaded
688 from the Genomic Data Commons website as clinical files and FPKM transcriptome-
689 sequencing files. For gene expression analysis, genes counts from the FPKM files were
690 assembled into a count matrix K_{ij} (for gene i in tumor sample j) after filtering genes with zero
691 geometric mean. Gene counts were normalized by calculating scaling factors analogous to
692 those calculated in the DESeq package [55, 56]:
693 λ_j=MEDIAN$_{i=1_to_17689}${K_{ij}/GEOMETRIC_MEAN$_{k=1_to_149}${K_{ik}}}. The normalized FPKM
694 value K_{ij}/λ_j was used as a measure of the expression level of gene i in tumor j. In the case of 5
695 patients for whom there were 2 sequencing files, we took the geometric mean value of
696 normalized gene counts. This normalization introduced in most cases only a small correction
697 (the average value of λ_j was λ=1.01 ± 0.12, mean ± s.d.; n=149) and was validated *a*
698 *posteriori* by the strong self-consistency of the results obtained. The cutoff value θ used to
699 categorize patients in cohorts with a low or high level of expression of a given gene in their
700 tumor, was chosen to maximize the statistical significance of the difference in survival
701 between the two cohorts of patients. For *BECN1* mRNA levels (8.56 ± 1.83 FPKM, mean ±
702 s.d., range: 4.2-18.0, n=124), a cutoff value of 8.895 FPKM was used throughout this study.

703 For *CCNA2* mRNA levels (4.76 ± 2.86 FPKM, mean ± s.d., range: 1.12-16.44, n=124) a
704 cutoff value of 5.66 FPKM was used throughout this study (see also **S2 file**).

705 The clinical data were verified by cross-referencing the various clinical files for the treatment
706 status and for the duration of patient survival without local or distant tumor recurrence. Only
707 the records of 124 of the 144 patients contained relevant indications on local recurrence and
708 the status of distant metastasis. They include 109 patients with a pancreas adenocarcinoma of
709 the ductal subtype, 6 with a Not Otherwise Stated subtype, 3 with a poorly differentiated and
710 1 with a well differentiated subtype, 3 with mixed phenotypes (ductal and micropapillary or
711 neuroendocrine subtypes) and 2 with an invasive phenotype. The "Initial treatment"
712 corresponded to removal of the primary tumor by partial or total pancreatectomy. Adjuvant
713 chemotherapy was recorded for 78% of patients (the treatment status was not specified for the
714 remaining patients) and this percentage increased to 89% for patients with distant metastasis-
715 free survival >360 day. When a patient had a local recurrence or a new cancer type, he was
716 censored at the time of that diagnostic in the Kaplan-Meier analysis for distant metastasis-free
717 survival. Data were processed and analyzed using Excel (version 16; Microsoft, USA)
718 upgraded with Real Statistics add-ins (Zaiontz, C., 2020, Real Statistics Using Excel.at
719 www.real-statistics.com) and GraphPad Prism version 5.00 (San Diego, California, USA).
720 Enrichment analysis was performed with Gene Set Enrichment Analysis software (GSEA
721 v4.2.0 for Windows and Mac) with default settings and the msigdb.v7.4.symbols.gmt dataset
722 available from the Broad Institute. Hierarchical gene clustering was performed using
723 Morpheus software (https://software.broadinstitute.org/morpheus). The references of
724 downloaded files and a synthetic summary of clinical data are given in **S2 file**. Normalized
725 sequencing data are provided in **S3 file**.

726

727 **Statistics:** In all graphs, each point corresponds to an independent measurement, the labels
728 above the data points indicate the average values and error bars are standard deviation unless
729 otherwise indicated. Significance was measured using a two-tailed Student's t-test unless
730 otherwise specified. Log-ranked (Mantel-Cox) and Fisher's exact probability test were
731 performed using GraphPad Prism version 5.00 or 8.00 (San Diego, California, USA).
732 Correlations were calculated using Excel software (Microsoft Standard Office 2016) and their
733 statistical significance calculated on the Vassar web site (http://vassarstats.net). Multivariate
734 Cox regression analysis was performed using Excel (version 16; Microsoft, USA) upgraded
735 with Real Statistics add-ins (Zaiontz, C., 2020, Real Statistics Using Excel.at www.real-
736 statistics.com). The number of * indicates the statistical significance of the difference between
737 the indicated mean values with * for $p<0.05$, ** for $p<10^{-2}$, *** for $p<10^{-3}$, **** for $p<10^{-4}$,
738 ***** for $p<10^{-5}$ and ******* for $p<10^{-6}$ and the same for #.

739

740 # Figure Legends

741 **Fig 1**: **Selection of pancreas cancer KC-DT66066 cells in SSQ at low cell density with**
742 **anticancer agents. A)** Outlines of clonogenic assays to assess the kinetics of SSQ formation.
743 Cells were plated at low cell density on day 0 (d0) and cultured as indicated. The labels on the
744 left are those used in the scatter plots. SSQi is a mixture of pharmacological agents that
745 reverts SSQ (see Methods). **B)** Kinetics of the generation of gemcitabine-resistant cells.
746 Scatter plots of cloning efficiency (CE) measured with the indicated clonogenic assays.
747 Labels in the red boxes indicate the percentage of seeded cells having formed a cell clone. *
748 indicates the statistical significance of the change in CE induced by SSQi supplementation
749 and # the statistical significance of the difference in CE between the indicated clonogenic
750 assays with SSQi supplementation. **C)** Representative pictures of fixed and stained cell

751 culture dishes after culturing the cells as indicated. **D)** Rationale for determining the initial
752 frequency of cancer cells in SSQ in a given cell population and the frequency at which they
753 are induced by cell subculture at low cell density or low cell density and low serum. The gem
754 d0 clonogenic assay selects cells that were already in SSQ in the initial cell population. The
755 selected SSQ cells switch to a proliferating state and formed cell clones after the addition of
756 SSQi (gem d0→ SSQi clonogenic assay). Growing cell clones obtained in clonogenic assays
757 with delayed gemcitabine selection and SSQi supplementation (gem d3→ SSQi and low
758 FCS→ gem d3→ SSQi) originated from cells already in SSQ in the initial population or that
759 were induced to enter SSQ by subculture at low cell density or at low cell density and in low
760 serum.

761

762 **Fig 2: SSQ induction in KC-DT66066 cells is enhanced by 3D cell preculture or**
763 **pretreatment with pharmacological inhibitors of mTOR in 2D cell cultures**. **A)** Growth
764 of cells seeded at 10^4 cells per well in cell-repellent surface 12-well plate and cultured for 10
765 days in regular growth medium supplemented with none (none) and 50% conditioned medium
766 (CM) from senescent mouse embryo fibroblasts cultures. The stars indicate the statistical
767 significance of the differences with cells grown in regular growth medium. Labels indicate
768 mean cell number. **B)** Representative pictures of cells grown for 7 days in cell-repellent
769 surface plates in regular growth medium supplemented with none (3D + none) or CM (3D +
770 CM). The scale bar indicates 0.25 mm. **C)** RT-qPCR analysis of mRNA species levels
771 according to the indicated cell-culture conditions. Stars indicate statistical significance of
772 differences with the KC-2D condition. 4 independent experiments were performed. **D)**
773 Clonogenic assays to compare SSQ induction in cells from 3D or 2D cultures using the same
774 cell dissociation method. Note that the relatively high frequency of cell clones in the
775 clonogenic assays gem d0→ none and low FCS→ gem d3→ none resulted from the

776 spontaneous reversion of cells in SSQ after gemcitabine selection when their frequency
777 exceeded 10% of the seeded cells. **E**) Schematic representation of the fusion protein encoded
778 by the reporter gene EGFP-LC3B-mRFP-LC3BΔG encoding the autophagy sensitive EGFP-
779 LC3B and the autophagy resistant mRFP-LC3ΔG fluorescent proteins. **F**) GFP to mRFP
780 fluorescence ratio in EGFP-LC3B-mRFP-LC3BΔG transduced cells cultured in 2D with
781 none, 100 nM bafilomycin A1 (baf1) or 200 nM Torin1 for 1 day or cultured in 3D with none
782 (3D+none) or CM (3D+CM) for 7 days. Stars indicate the significance of the difference with
783 untreated 2D-cultured (control) cells. **G**) Data from a representative flow cytometry
784 experiment showing the distribution of the ratio of GFP to mRFP fluorescence in transduced
785 cells cultured as indicated. **H)** Clonogenic assays to compare SSQ induction in cells
786 pretreated at medium cell density in 2D-cultures with none or 200 nM Torin1 for 1 day
787 (pretreatment) before cell passaging at low density. Labels indicate the percentage of seeded
788 cells having formed a cell clone after SSQi supplementation. Stars indicate statistical
789 significance of differences with 2D control in panel **D** and with untreated cells in panel **H** in
790 clonogenic tests with SSQi supplementation.

791

792 **Fig 3: Beclin-1 downregulation inhibits SSQ but not autophagy. A)** and **B)** clonogenic
793 assays to compare SSQ induction in KC-DT66066 cell populations transduced with shRNA
794 targeting GFP (KCsh*gfp*) or Beclin-1 (KCsh*becn1*) and pretreated with none **(A**) or 200 nM
795 Torin1 (**B**) as depicted in Fig 2H. Labels above bars indicate the percentage of seeded cells
796 having formed a cell clone after SSQi supplementation. * indicate statistical significance of
797 CE differences after SSQi supplementation between KCsh*gfp* and KCsh*becn1* cells. **C**)
798 Western Blot analysis of KCsh*gfp* and KCsh*Becn1* cell populations seeded at medium cell
799 density at d0 and treated from d1 to d2 as indicated (baf1 and tor1 were for 100 nM
800 bafilomycin A1 and 200 nM Torin1 respectively). This is one representative western blot of 3

801 analyzed. The arrow indicates the SQSTM1 band and the star a non-specific band. **D**) *left*:
802 GFP/mRFP fluorescence ratio showing no difference in autophagic flux in KC*shgfp* and
803 KC*shbecn1* cell populations transduced with the EGFP-LC3B-mRFP-LC3BΔG reporter gene.
804 Cells were passaged at medium cell density at d0, treated from d1 to d2 with the indicated
805 drugs (none, bafilomycin A1 (baf1), and/or Torin1) and analyzed as in Fig 2F-G. Dotted lines
806 connect data points derived from a same experiment. Labels indicate the number of
807 independent reporter gene transduction experiments. *Right*: A representative flow cytometry
808 experiment shown.

809

810 **Fig 4: KC-DT66066 cells in SSQ are distinguished from senescent cells and exhibit**
811 **morphological characteristics of Epithelial to Mesenchymal Transition (EMT). A**)
812 Outlines of cancer cell tracking in the low FCS→ gem d3→SSQi clonogenic assay using a
813 phase contrast microscope to identify cancer cells in SSQ. Cells were pretreated for 1 day
814 with 200 nM Torin1 at medium cell density before seeding at low cell density and in low
815 serum at day 0 (d0). The cancer cells in SSQ were identified *a posteriori* as individual cells at
816 the end of gemcitabine selection (at d7) having given rise to a cell clone after culture in
817 growth medium supplemented with SSQi. **B)** Representative pictures of clonogenic cancer
818 cells in SSQ (upper row) and non-clonogenic cancer cells (lower row) photographed on day 7.
819 **C)** Scatter plots showing greater nuclear and cellular size in non-clonogenic cells at day 7
820 compared to SSQ cells. A total of 186 cells were analyzed in two independent experiments.
821 **D)** RT-qPCR analysis of mRNA species levels in SSQ-enriched cell populations (SSQ; n=4)
822 versus growing cell populations (Exp; n=2) and senescent cell populations (Sen; n=2). SSQ-
823 enriched cell populations were Torin1-pretreated cells from the low FCS→ gem d3
824 clonogenic assay analyzed at day 7. Senescent cells populations were derived by culturing
825 cells at medium cell density with gemcitabine plus SSQi for about 10 days and further

826 culturing for 1 day in regular medium before cell lysis. Stars indicate statistical significance
827 of the differences with SSQ-enriched cell populations using a two tailed heteroscedastic
828 student's t test. **E)** Representative pictures of cancer cells in SSQ on day 7 that have
829 transitioned to an epithelial phenotype by day 10 (upper row), day 14 (middle row) or have
830 maintained a mesenchymal phenotype by day 14 (lower pictures row).

831

832 **Fig 5: SSQ regulates tumor development. A**) Outlines of the experiment performed to
833 compare tumorigenicity of KC-DT66066 cells in a proliferating state or in SSQ. **B)** Tumor
834 growth curves in individual NOD-SCID mice subcutaneously injected with proliferating KC-
835 DT66066 cells (Exp group, n=6) or with cells in SSQ and treated with none (Ssq / none
836 group, n=4) or gemcitabine (Ssq / gem group; n=4). **C**) and **D**) Scatter plots showing the time
837 taken for tumors to reach a volume of 10 mm^3 (**C**) or 100 mm^3 (**D**). p indicates the statistical
838 significance of the difference in the proportion of mice with a slow tumor growth rate as
839 calculated with a Fisher's exact probability test. Note that a third tumor in the Ssq/none group
840 showed a slow tumor growth rate but only after having reached 200 mm^3 (see Fig 5B and
841 main text). **E**) Growing tumors contain a significant percentage of cancer cells in SSQ or
842 prone to enter SSQ. Clonogenic assays using cells dissociated from growing tumor resected
843 from mice in the Exp (n=1), Ssq/none (n=2) and Ssq/gem (n=2) groups and directly tested for
844 SSQ as described in Fig 1A. Data were normalized to 100% of cloning efficiency in the none
845 → SSQi clonogenic assay. * indicates the statistical significance of the change in CE induced
846 by SSQi supplementation. Note that spontaneous reversion of SSQ (that could be observed
847 with the clonogenic assay low FCS → gem d3→ none) strongly increased in some dishes
848 containing a high absolute number of cells in SSQ as observed in Fig 2D.

849

850 **Fig 6: Elevated Beclin-1 expression in the primary tumor of PAAD patients is associated**
851 **with an increased rate of metastasis in the patient cohort with a metastasis-free survival**
852 **greater than 360 days. A)** Kaplan-Meier curves for distant metastasis-free survival in PAAD
853 patients according to the level of Beclin-1 transcripts in their primary tumor. **B)** Same as **(A)**
854 but restricted to patients with survival time greater than 360 days. Initial treatment was partial
855 or total pancreatectomy to remove the tumor and at least 78% of patients received adjuvant
856 pharmaceutical treatments (see **S2 file**). Significance (p) of the difference in survival and
857 hazard ratio (HR) were calculated with a Mantel-Cox Log-ranked test. **C)** Gene set
858 enrichment analysis (GSEA) showing significant enrichment for hallmarks of MYC,
859 mTORC1 and unfolded protein response signaling activity [57] in primary tumors of PAAD
860 patients with a distant-metastasis-free survival time less than 360 days after initial treatment
861 (n=60) *versus* greater than 360 days (n=64). Normalized enrichment score (NES), its
862 statistical significance (p) and its false discovery rate (FDR) are indicated.

863

864 **Fig 7: Cyclin A2 marks tumors with elevated mTORC1 activity and combines with**
865 **Beclin-1 to predict kinetics of metastases development. A)** Kaplan-Meier curves for
866 distant metastasis-free survival in PAAD patients with high or low level of Cyclin A2
867 (*CCNA2*) transcripts in their primary tumor. **B)** GSEA demonstrates significant enrichment
868 for hallmarks of cell proliferation and mTORC1 signaling [57] in the primary tumors of PAAD
869 patients with high level (n=31) versus low level (n=93) of *CCNA2* transcripts. Normalized
870 enrichment score (NES), its statistical significance (p) and its false discovery rate (FDR) are
871 indicated. **C**) Hierarchical clustering of genes according to the Pearson correlation of their
872 transcription levels in the primary tumors of PAAD patients (n=124). The colors indicate the
873 value of the Pearson correlation coefficient for a given gene pair, ranging from -1 (blue) to +1
874 (red). The mTORC1 genes markers correspond to the first 15 highest ranked genes composing

875 the mTORC1 signaling signature derived by GSEA analysis of PAAD tumors in Fig 6C (gene
876 set M5924; [57]). **D)** Kaplan-Meier curves for distant metastasis-free survival in PAAD patients
877 with survival time less than 360 days according to the transcript levels of cyclin A2 (CCNA2)
878 and Beclin 1 (BCEN1) in their primary tumor. **E)** Same as panel D), but limited to patients
879 with a survival time greater than 360 days. Log-ranked (Mantel-Cox) test was used to
880 calculate the statistical significance (p) of the differences in distant metastasis-free survival
881 between adjacent survival curves and hazard ratios (HR).

882

883 **Fig 8: A molecular model of self-sustained quiescence.** mTORC1 is a central node in the
884 regulatory network controlling cell proliferation, for instance by regulating c-Myc activity,
885 cyclin D accumulation and protein synthesis. Activation of Beclin-1 by downregulation of
886 mTORC1 activity leads to activation of a regulatory loop (red circle in right panel) that helps
887 to maintain a low mTORC1 activity. Indeed, Beclin-1 induced the degradation of cell surface
888 receptor for growth factors and iron (transferrin receptor), and directly inhibits the Xc^-
889 cystine/glutamate antiporter [17, 30-33], which inhibits mTOR activity via nutrient depletion,
890 oxidative stress and suppression of growth factors signaling pathways [35, 38, 40-45]. Note that
891 BMP signaling stabilizes SSQ in prostate cancer cells [8, 10] but appears to play a minor role in
892 PAAD cells (see Methods for details and data not shown). EMT possibly favors the entry in
893 SSQ and MET the maintenance of the proliferating state. The bold corresponds to activated
894 signaling pathways while the dotted line corresponds to repressed pathways

895

Declarations and ethics satements

Ethical approval: The animal protocol used in this study was reviewed and approved by the local ethics committee (Comité d'Ethique en Expérimentation Animale of University of Paris; approved protocol CEEA 18-088 submitted by C. Nicco and T. Tchenio). Animals received humane care in compliance with the guidelines implemented at our institution (INSERM and University Paris Descartes).

Data availability statement for Share Upon Reasonable Request Data: The authors declare that all data supporting the findings of this study are available within the article and its appendices, or available from the corresponding author upon reasonable request.

Competing interests: The authors have declared that no conflict of interest exists.

Funding: No grant funded this study.

Author contributions: Conceptualization: TT. Supervision: CN, FB, TT. Methodology: TT. Investigation: JG provided murine pancreas cancer cell lines derived from corresponding transgenic mice; MH carried out counting of colonies from clonogenic assays and plasmids constructions in studies with prostate cancer cells. TT performed all cell culture, flow cytometry, qPCR, Western Blot experiments and analysis of patients' records; CN and MT carried out animal experiments. Formal analysis: T.T; Analysis and Visualization of Data:

917 FB, CN, TT. Writing original draft: TT. Review and Editing: CN, FB, FD, FLT, JG, LD and
918 TT.

919

920 # References

921 1. Luzzi KJ, MacDonald IC, Schmidt EE, Kerkvliet N, Morris VL, Chambers AF,
922 Groom AC. Multistep nature of metastatic inefficiency: dormancy of solitary cells after
923 successful extravasation and limited survival of early micrometastases. The American journal
924 of pathology 1998; 153:865-73.
925 2. Cameron MD, Schmidt EE, Kerkvliet N, Nadkarni KV, Morris VL, Groom AC,
926 Chambers AF, MacDonald IC. Temporal progression of metastasis in lung: cell survival,
927 dormancy, and location dependence of metastatic inefficiency. Cancer research 2000;
928 60:2541-6.
929 3. Naumov GN, MacDonald IC, Weinmeister PM, Kerkvliet N, Nadkarni KV, Wilson
930 SM, Morris VL, Groom AC, Chambers AF. Persistence of solitary mammary carcinoma cells
931 in a secondary site: a possible contributor to dormancy. Cancer research 2002; 62:2162-8.
932 4. McAllister SS, Gifford AM, Greiner AL, Kelleher SP, Saelzler MP, Ince TA,
933 Reinhardt F, Harris LN, Hylander BL, Repasky EA, et al. Systemic endocrine instigation of
934 indolent tumor growth requires osteopontin. Cell 2008; 133:994-1005.
935 5. Risson E, Nobre AR, Maguer-Satta V, Aguirre-Ghiso JA. The current paradigm and
936 challenges ahead for the dormancy of disseminated tumor cells. Nat Cancer 2020; 1:672-80.
937 6. Shen S, Vagner S, Robert C. Persistent Cancer Cells: The Deadly Survivors. Cell
938 2020; 183:860-74.

939 7. Janni W, Rack B, Schindlbeck C, Strobl B, Rjosk D, Braun S, Sommer H, Pantel K,
940 Gerber B, Friese K. The persistence of isolated tumor cells in bone marrow from patients with
941 breast carcinoma predicts an increased risk for recurrence. Cancer 2005; 103:884-91.
942 8. Bui AT, Laurent F, Havard M, Dautry F, Tchenio T. SMAD signaling and redox
943 imbalance cooperate to induce prostate cancer cell dormancy. Cell cycle 2015; 14:1218-31.
944 9. Havard M, Dautry F, Tchenio T. A dormant state modulated by osmotic pressure
945 controls clonogenicity of prostate cancer cells. The Journal of biological chemistry 2011;
946 286:44177-86.
947 10. Bui AT, Huang ME, Havard M, Laurent-Tchenio F, Dautry F, Tchenio T. Transient
948 exposure to androgens induces a remarkable self-sustained quiescent state in dispersed
949 prostate cancer cells. Cell cycle 2017; 16:879-93.
950 11. Baer R, Cintas C, Dufresne M, Cassant-Sourdy S, Schonhuber N, Planque L, Lulka H,
951 Couderc B, Bousquet C, Garmy-Susini B, et al. Pancreatic cell plasticity and cancer initiation
952 induced by oncogenic Kras is completely dependent on wild-type PI 3-kinase p110alpha.
953 Genes & development 2014; 28:2621-35.
954 12. Hingorani SR, Petricoin EF, Maitra A, Rajapakse V, King C, Jacobetz MA, Ross S,
955 Conrads TP, Veenstra TD, Hitt BA, et al. Preinvasive and invasive ductal pancreatic cancer
956 and its early detection in the mouse. Cancer Cell 2003; 4:437-50.
957 13. Maciel-Baron LA, Morales-Rosales SL, Aquino-Cruz AA, Triana-Martinez F, Galvan-
958 Arzate S, Luna-Lopez A, Gonzalez-Puertos VY, Lopez-Diazguerrero NE, Torres C,
959 Konigsberg M. Senescence associated secretory phenotype profile from primary lung mice
960 fibroblasts depends on the senescence induction stimuli. Age (Dordrecht, Netherlands) 2016;
961 38:26.

962 14. Fung C, Lock R, Gao S, Salas E, Debnath J. Induction of autophagy during
963 extracellular matrix detachment promotes cell survival. Molecular biology of the cell 2008;
964 19:797-806.
965 15. Kaizuka T, Morishita H, Hama Y, Tsukamoto S, Matsui T, Toyota Y, Kodama A,
966 Ishihara T, Mizushima T, Mizushima N. An Autophagic Flux Probe that Releases an Internal
967 Control. Molecular cell 2016; 64:835-49.
968 16. Thoreen CC, Kang SA, Chang JW, Liu Q, Zhang J, Gao Y, Reichling LJ, Sim T,
969 Sabatini DM, Gray NS. An ATP-competitive mammalian target of rapamycin inhibitor
970 reveals rapamycin-resistant functions of mTORC1. The Journal of biological chemistry 2009;
971 284:8023-32.
972 17. Wirawan E, Lippens S, Vanden Berghe T, Romagnoli A, Fimia GM, Piacentini M,
973 Vandenabeele P. Beclin1: a role in membrane dynamics and beyond. Autophagy 2012; 8:6-
974 17.
975 18. Hosokawa N, Hara T, Kaizuka T, Kishi C, Takamura A, Miura Y, Iemura S, Natsume
976 T, Takehana K, Yamada N, et al. Nutrient-dependent mTORC1 association with the ULK1-
977 Atg13-FIP200 complex required for autophagy. Molecular biology of the cell 2009; 20:1981-
978 91.
979 19. Di Bartolomeo S, Corazzari M, Nazio F, Oliverio S, Lisi G, Antonioli M, Pagliarini V,
980 Matteoni S, Fuoco C, Giunta L, et al. The dynamic interaction of AMBRA1 with the dynein
981 motor complex regulates mammalian autophagy. The Journal of cell biology 2010; 191:155-
982 68.
983 20. Vadlakonda L, Dash A, Pasupuleti M, Anil Kumar K, Reddanna P. The Paradox of
984 Akt-mTOR Interactions. Frontiers in oncology 2013; 3:165.

985 21. Mauvezin C, Neufeld TP. Bafilomycin A1 disrupts autophagic flux by inhibiting both
986 V-ATPase-dependent acidification and Ca-P60A/SERCA-dependent autophagosome-
987 lysosome fusion. Autophagy 2015; 11:1437-8.
988 22. Rocchi A, Yamamoto S, Ting T, Fan Y, Sadleir K, Wang Y, Zhang W, Huang S,
989 Levine B, Vassar R, et al. A Becn1 mutation mediates hyperactive autophagic sequestration
990 of amyloid oligomers and improved cognition in Alzheimer's disease. PLoS genetics 2017;
991 13:e1006962.
992 23. Mitsui Y, Schneider EL. Increased nuclear sizes in senescent human diploid fibroblast
993 cultures. Experimental cell research 1976; 100:147-52.
994 24. Nakajima T, Nakashima T, Okada Y, Jo M, Nishikawa T, Mitsumoto Y, Katagishi T,
995 Kimura H, Itoh Y, Kagawa K, et al. Nuclear size measurement is a simple method for the
996 assessment of hepatocellular aging in non-alcoholic fatty liver disease: Comparison with
997 telomere-specific quantitative FISH and p21 immunohistochemistry. Pathology international
998 2010; 60:175-83.
999 25. Hernandez-Segura A, Nehme J, Demaria M. Hallmarks of Cellular Senescence.
1000 Trends in cell biology 2018; 28:436-53.
1001 26. Deshmukh SK, Tyagi N, Khan MA, Srivastava SK, Al-Ghadhban A, Dugger K, Carter
1002 JE, Singh S, Singh AP. Gemcitabine treatment promotes immunosuppressive
1003 microenvironment in pancreatic tumors by supporting the infiltration, growth, and
1004 polarization of macrophages. Sci Rep 2018; 8:12000.
1005 27. Cianfanelli V, Fuoco C, Lorente M, Salazar M, Quondamatteo F, Gherardini PF, De
1006 Zio D, Nazio F, Antonioli M, D'Orazio M, et al. AMBRA1 links autophagy to cell
1007 proliferation and tumorigenesis by promoting c-Myc dephosphorylation and degradation.
1008 Nature cell biology 2015; 17:20-30.

1009 28. Maiani E, Milletti G, Nazio F, Holdgaard SG, Bartkova J, Rizza S, Cianfanelli V,
1010 Lorente M, Simoneschi D, Di Marco M, et al. AMBRA1 regulates cyclin D to guard S-phase
1011 entry and genomic integrity. Nature 2021; 592:799-803.
1012 29. Simoneschi D, Rona G, Zhou N, Jeong YT, Jiang S, Milletti G, Arbini AA, O'Sullivan
1013 A, Wang AA, Nithikasem S, et al. CRL4(AMBRA1) is a master regulator of D-type cyclins.
1014 Nature 2021; 592:789-93.
1015 30. Thoresen SB, Pedersen NM, Liestol K, Stenmark H. A phosphatidylinositol 3-kinase
1016 class III sub-complex containing VPS15, VPS34, Beclin 1, UVRAG and BIF-1 regulates
1017 cytokinesis and degradative endocytic traffic. Experimental cell research 2010; 316:3368-78.
1018 31. Rohatgi RA, Janusis J, Leonard D, Bellve KD, Fogarty KE, Baehrecke EH, Corvera S,
1019 Shaw LM. Beclin 1 regulates growth factor receptor signaling in breast cancer. Oncogene
1020 2015; 34:5352-62.
1021 32. Matthew-Onabanjo AN, Janusis J, Mercado-Matos J, Carlisle AE, Kim D, Levine F,
1022 Cruz-Gordillo P, Richards R, Lee MJ, Shaw LM. Beclin 1 Promotes Endosome Recruitment
1023 of Hepatocyte Growth Factor Tyrosine Kinase Substrate to Suppress Tumor Proliferation.
1024 Cancer research 2020; 80:249-62.
1025 33. Song X, Zhu S, Chen P, Hou W, Wen Q, Liu J, Xie Y, Liu J, Klionsky DJ, Kroemer
1026 G, et al. AMPK-Mediated BECN1 Phosphorylation Promotes Ferroptosis by Directly
1027 Blocking System Xc(-) Activity. Current biology : CB 2018; 28:2388-99 e5.
1028 34. Hu F, Li G, Huang C, Hou Z, Yang X, Luo X, Feng Y, Wang G, Hu J, Cao Z. The
1029 autophagy-independent role of BECN1 in colorectal cancer metastasis through regulating
1030 STAT3 signaling pathway activation. Cell death & disease 2020; 11:304.
1031 35. Reiling JH, Sabatini DM. Stress and mTORture signaling. Oncogene 2006; 25:6373-
1032 83.

1033 36. Galvez T, Teruel MN, Heo WD, Jones JT, Kim ML, Liou J, Myers JW, Meyer T.
1034 siRNA screen of the human signaling proteome identifies the PtdIns(3,4,5)P3-mTOR
1035 signaling pathway as a primary regulator of transferrin uptake. Genome Biol 2007; 8:R142.
1036 37. Ohyashiki JH, Kobayashi C, Hamamura R, Okabe S, Tauchi T, Ohyashiki K. The oral
1037 iron chelator deferasirox represses signaling through the mTOR in myeloid leukemia cells by
1038 enhancing expression of REDD1. Cancer science 2009; 100:970-7.
1039 38. Alexander A, Cai SL, Kim J, Nanez A, Sahin M, MacLean KH, Inoki K, Guan KL,
1040 Shen J, Person MD, et al. ATM signals to TSC2 in the cytoplasm to regulate mTORC1 in
1041 response to ROS. Proceedings of the National Academy of Sciences of the United States of
1042 America 2010; 107:4153-8.
1043 39. Bayeva M, Khechaduri A, Puig S, Chang HC, Patial S, Blackshear PJ, Ardehali H.
1044 mTOR regulates cellular iron homeostasis through tristetraprolin. Cell metabolism 2012;
1045 16:645-57.
1046 40. Watson A, Lipina C, McArdle HJ, Taylor PM, Hundal HS. Iron depletion suppresses
1047 mTORC1-directed signalling in intestinal Caco-2 cells via induction of REDD1. Cellular
1048 signalling 2016; 28:412-24.
1049 41. Pant K, Saraya A, Venugopal SK. Oxidative stress plays a key role in butyrate-
1050 mediated autophagy via Akt/mTOR pathway in hepatoma cells. Chemico-biological
1051 interactions 2017; 273:99-106.
1052 42. Oka SI, Hirata T, Suzuki W, Naito D, Chen Y, Chin A, Yaginuma H, Saito T,
1053 Nagarajan N, Zhai P, et al. Thioredoxin-1 maintains mechanistic target of rapamycin (mTOR)
1054 function during oxidative stress in cardiomyocytes. The Journal of biological chemistry 2017;
1055 292:18988-9000.
1056 43. Romero AM, Ramos-Alonso L, Montella-Manuel S, Garcia-Martinez J, de la Torre-
1057 Ruiz MA, Perez-Ortin JE, Martinez-Pastor MT, Puig S. A genome-wide transcriptional study

1058 reveals that iron deficiency inhibits the yeast TORC1 pathway. Biochim Biophys Acta Gene
1059 Regul Mech 2019; 1862:194414.
1060 44. Daher B, Parks SK, Durivault J, Cormerais Y, Baidarjad H, Tambutte E, Pouyssegur J,
1061 Vucetic M. Genetic Ablation of the Cystine Transporter xCT in PDAC Cells Inhibits
1062 mTORC1, Growth, Survival, and Tumor Formation via Nutrient and Oxidative Stresses.
1063 Cancer research 2019; 79:3877-90.
1064 45. Zhou J, Li XY, Liu YJ, Feng J, Wu Y, Shen HM, Lu GD. Full-coverage regulations of
1065 autophagy by ROS: from induction to maturation. Autophagy 2021:1-16.
1066 46. Almog N. Molecular mechanisms underlying tumor dormancy. Cancer Lett 2010;
1067 294:139-46.
1068 47. Cianfanelli V, D'Orazio M, Cecconi F. AMBRA1 and BECLIN 1 interplay in the
1069 crosstalk between autophagy and cell proliferation. Cell cycle 2015; 14:959-63.
1070 48. Liang XH, Jackson S, Seaman M, Brown K, Kempkes B, Hibshoosh H, Levine B.
1071 Induction of autophagy and inhibition of tumorigenesis by beclin 1. Nature 1999; 402:672-6.
1072 49. Wechman SL, Pradhan AK, DeSalle R, Das SK, Emdad L, Sarkar D, Fisher PB. New
1073 Insights Into Beclin-1: Evolution and Pan-Malignancy Inhibitor Activity. Advances in cancer
1074 research 2018; 137:77-114.
1075 50. Kim HS, Lee SH, Do SI, Lim SJ, Park YK, Kim YW. Clinicopathologic correlation of
1076 beclin-1 expression in pancreatic ductal adenocarcinoma. Pathol Res Pract 2011; 207:247-52.
1077 51. Song S, Wang B, Gu S, Li X, Sun S. Expression of Beclin 1 and Bcl-2 in pancreatic
1078 neoplasms and its effect on pancreatic ductal adenocarcinoma prognosis. Oncology letters
1079 2017; 14:7849-61.
1080 52. Takahashi Y, Coppola D, Matsushita N, Cualing HD, Sun M, Sato Y, Liang C, Jung
1081 JU, Cheng JQ, Mule JJ, et al. Bif-1 interacts with Beclin 1 through UVRAG and regulates
1082 autophagy and tumorigenesis. Nature cell biology 2007; 9:1142-51.

1083 53. Vera-Ramirez L, Vodnala SK, Nini R, Hunter KW, Green JE. Autophagy promotes
1084 the survival of dormant breast cancer cells and metastatic tumour recurrence. Nature
1085 communications 2018; 9:1944.
1086 54. Sancak Y, Peterson TR, Shaul YD, Lindquist RA, Thoreen CC, Bar-Peled L, Sabatini
1087 DM. The Rag GTPases bind raptor and mediate amino acid signaling to mTORC1. Science
1088 (New York, NY) 2008; 320:1496-501.
1089 55. Anders S, Huber W. Differential expression analysis for sequence count data. Nature
1090 Precedings 2010.
1091 56. Dillies MA, Rau A, Aubert J, Hennequet-Antier C, Jeanmougin M, Servant N, Keime
1092 C, Marot G, Castel D, Estelle J, et al. A comprehensive evaluation of normalization methods
1093 for Illumina high-throughput RNA sequencing data analysis. Brief Bioinform 2013; 14:671-
1094 83.
1095 57. Liberzon A, Birger C, Thorvaldsdottir H, Ghandi M, Mesirov JP, Tamayo P. The
1096 Molecular Signatures Database (MSigDB) hallmark gene set collection. Cell Syst 2015;
1097 1:417-25.

1098

1099

1100 Appendices

1101 **Fig S1: Selection of cancer cells in SSQ with anticancer agents in pancreas and prostate**
1102 **cancer cell lines cultured at clonogenic cell density**. **A**) Delayed addition of SSQi after
1103 gemcitabine selection does not impact recovery of growing cell clones. Pictures of KC-
1104 DT66066 cell culture dishes from a representative experiment (of 3) fixed and stained after
1105 cell culture as indicated. **B**) Selection of cancer cells in SSQ with gemcitabine using indicated
1106 pancreas cancer cell lines derived from KC and KPC mouse models. **C)** Representative

1107 pictures showing the formation of spheroid-like structures in KC-A338 but not KC-DT66066
1108 cells cultured in 2D. Scaling bar indicates 1 mm. **D**) Comparison of the selection of KC-
1109 DT66066 cell in SSQ with 100 nM nocodazole (noco), 30 ng/mL gemcitabine (gem) and 100
1110 ng/mL vincristine (vin). **E**) Selection of SSQ in LNCaP* cells using doxorubicine (dox) and
1111 Docetaxel (Tx) at the indicated concentrations. Note that cells were selected from day 0 to
1112 day 8 (d0-d8), washed and further cultured for around 20 days in regular growth medium
1113 supplemented with none or SSQi. Labels indicates the percentage of seeded cells having
1114 formed a cell clone after supplementation with SSQi. **F)** clonogenic assays for testing
1115 induction of SSQ in KC-DT66066 cell populations generated after one SSQ
1116 induction/selection/reversal cycle using gemcitabine (n=2) or nocodazole (n=2) to select cells
1117 in SSQ. Cell populations were derived from experiments depicted in Fig S1D. Stars indicate
1118 statistical significance of cloning efficiency differences between cells untreated and treated
1119 with SSQi after drug selection.

1120

1121 **Fig S2: SSQ induction is regulated by mTOR and Beclin-1 but not autophagic flux**. **A**)
1122 Increased frequency of C4-2 cells in SSQ induced by treatment with 200 nM Torin1 from day
1123 1 to day 3 (torin1 d1-d3; cells were seeded at low cell density on day 0). **B**) Increased
1124 frequency of KC-DT66066 cells in SSQ induced by treatment of cells with 5 nM rapamycin
1125 from day 0 to day 3 (rap d0-d3; cells were seeded at low cell density on day 0). **C)**
1126 Downregulation of Beclin-1 expression significantly decreases frequency of SSQ cells in KC-
1127 A338 cell populations. Cell populations transduced with sh*gfp* (control) or sh*Becn1*
1128 expressing vectors were assayed with the gem d0 clonogenic assay as described in Fig. 1. **D**)
1129 No significant effect of autophagy inhibitor bafilomycin A1 on SSQ induction by Torin1.
1130 Native KC-DT66066 cells were pretreated at medium cell density with none (no
1131 pretreatment), 100 nM bafilomycin A1 (baf1 pre-treatment), 200 nM Torin1 (tor1

1132 pretreatment), or bafilomycin A1 + Torin1 (baf1+tor1 pretreatment) for 1 day prior to cell
1133 seeding at low cell density for assaying SSQ induction. Note that bafilomycin A1 induced
1134 delayed toxicity (compare CE in the "none" clonogenic assays for the different pretreatment
1135 groups) that at least partially explained the non-significant difference in SSQ induction
1136 between the tor1 and baf1+tor1 pretreatment groups. **E)** Same as D) but performed in human
1137 C4-2 cells. Cells were seeded at low density on day 0 and treated as indicated from day 2 to 3
1138 before gemcitabine selection. It is one of 2 experiments done with either Torin1 or rapamycin.
1139 **F)** Western Blot analysis of KC-DT66066 transduced with empty (control) or HA-*Becn1*^{F121A}-
1140 expressing retroviral vectors. Note the higher molecular weight of HA-BECN1^{F121A} compared
1141 to wild type (wt) BECN1. **G)** Comparison of autophagic flux between control and HA-
1142 *Becn1*^{F121A}-transduced cell populations cultured at medium cell density and treated as
1143 indicated for one day before cytometric analysis to measure gfp/mRFP fluorescence ratio. 4
1144 independent cell populations were generated by superinfection with MRX-IP-GFP-LC3-RFP-
1145 LC3ΔG retroviral expression vector and assayed for autophagic flux 4 days later. **H)** Similar
1146 rate of SSQ induction in control or HA-*Becn1*^{F121A}-transduced cell populations as assayed
1147 with the indicated clonogenic assays. Labels indicates the percentage of seeded cells that
1148 formed a cell clone after SSQi supplementation.

1149

1150 **Fig S3: Tumorigenicity of KC cells injected subcutaneously in mice. A**) Tumor growth
1151 curves in allogenic C57Bl/6 mice injected subcutaneously with 10^6 KCsh*gfp* or KCsh*Becn1*
1152 cells. The errors bars correspond to the standard error of the mean. * indicates statistically
1153 significant differences ($p<0.05$) between the 2 groups of mice. **B)** Same as A but mice were
1154 treated once with gemcitabine (100 mg/kg i.p.) on day 4 after cell injection. **C**) Comparison of
1155 cell proliferation between KC*sghgfp* and KC*shbecn1* cell populations (3 independent pairs)
1156 seeded à $4x10^5$ cells in 6 cm diameter dish and cultured for 2 days in regular growth medium

1157 before cell counting. **D**) Tumor growth curves of individual NOD-SCID mice injected with
1158 10^2 and 10^3 dissociated KC-DT66066 cells harvested from growing 2D cell-cultures. **E**)
1159 Comparison of mRNA species levels in growing tumors derived from indolent tumors (n=5 in
1160 blue) to those measured in Exp* group tumors (n=4 in red) and in KC-DT66066 cells cultured
1161 in 2D at medium cell density (in black, normalized to 1 as in Figure 2C and File S1). Labels
1162 in black indicate number of independent experiments for growing KC-DT66066 cells in 2D-
1163 culture. * indicates the statistical significance of the differences between tumors and KC-
1164 DT66066 cells in 2D-culture.

1165

1166 **Fig S4: Beclin-1 and Cyclin A2 transcript levels in the primary tumor of PAAD patients**
1167 **are predictive of early and late metastasis. A)** Kaplan-Meier curves for distant metastasis-
1168 free survival restricted to PAAD patients with T3-N1-M0/Mx clinical grade and according to
1169 the level of Beclin-1 transcripts in their primary tumor. Statistical difference (p) in survival
1170 and hazard ratio (HR) are indicated. B) Same as panel A but also restricted to patients with
1171 distant metastasis-free survival time greater than 360 days. C) Miscellaneous gene set
1172 enrichments also found in primary tumors of PAAD patients with distant metastasis-free
1173 survival time less than 360 days after initial treatment (n=60) *versus* greater than 360 days
1174 (n=64). Normalized enrichment score (NES), its statistical significance (p) and its false
1175 discovery rate (FDR) are indicated. D) Kaplan-Meier curves for distant metastasis-free
1176 survival restricted to PAAD patients with T3-N1-M0/Mx clinical grade and according to the
1177 level of Cyclin A2 (CCNA2) transcripts in their primary tumor. E) Gene set enrichment found
1178 in the primary tumors of PAAD patients with high level (n=31) *versus* low level (n=93) of
1179 CCNA2 transcripts. F) Pearson's correlation coefficient between Beclin-1 or Cyclin A2
1180 transcript levels and those of cancer, mesenchymal, endothelial, and immune cell marker

1181 genes in primary tumors of PAAD patients (n=124). The stars indicate the statistical
1182 significance of the correlation.

1183

1184 **S1 file:** Sequences of primers used for RT-qPCR analysis and synthetic summary of RT-
1185 qPCR expression data.

1186

1187 **S2 file:** Synthetic summary of clinical and sequencing data including references of clinical
1188 and sequencing files retrieved from the Genomic Data Commons website.

1189

1190 **S3 file:** Genes count matrix derived from the 149 FPKM sequencing files (retrieved from the
1191 Genomic Data Commons website) and normalized by scaling factors λ_{ij}. See the Materials
1192 and Methods section for further explanations.

1193

Table 1: **Most clonogenic KC-DT66066 cells in SSQ are small spindle-shaped cells.**

Clonogenic status[a] **(number of cells)**	**Small spindle-shaped**	**Rounded**	**Senescent-like**[b]	**Miscellaneous**[c]
***Clonogenic cells in SSQ* (n=29)**	18	6	1	4
***Non-clonogenic cells* (n=157)**	26	48	58	25
Fisher's exact test[d]	-	<0.0001	<0.0001	0.01

[a] assessed at the 15th day of the low FCS→ gem→ SSQi clonogenic assay.
[b] large and flattened morphology.
[c] mostly multipolar cells.
[d] Statistical significance of the difference in the repartition of small spindle-shaped cells and cells of the indicated morphology between clonogenic cancer cells in SSQ and non-clonogenic cancer cells observed at the last day of gemcitabine selection (day 7).

Table 2: **Early and late (before and after 360 days, respectively) distant metastases events recorded in T3N1M0/x PAAD patients according to their primary tumor phenotype.**

primary tumor phenotype (number of patients)	SSQ competence	Early metastases events[a]	Late metastases events[b]	Fisher's exact test[c]
CCNA2^{high} **(n=20)**	low	8	2	0.0007
CCNA2^{low} BECN1^{low} **(n=41)**	low	10	4	0.0016
CCNA2^{low} BECN1^{high} **(n=18)**	high	0	9	-

[a] within 360 days of initial treatment.
[b] beyond 360 days after initial treatment
[c] Statistical significance of the difference in the repartition of early and late metastases events compared to the cohort of patients with a *CCNA2*^{low} *BECN1*^{high} tumor phenotype.

Figure 1

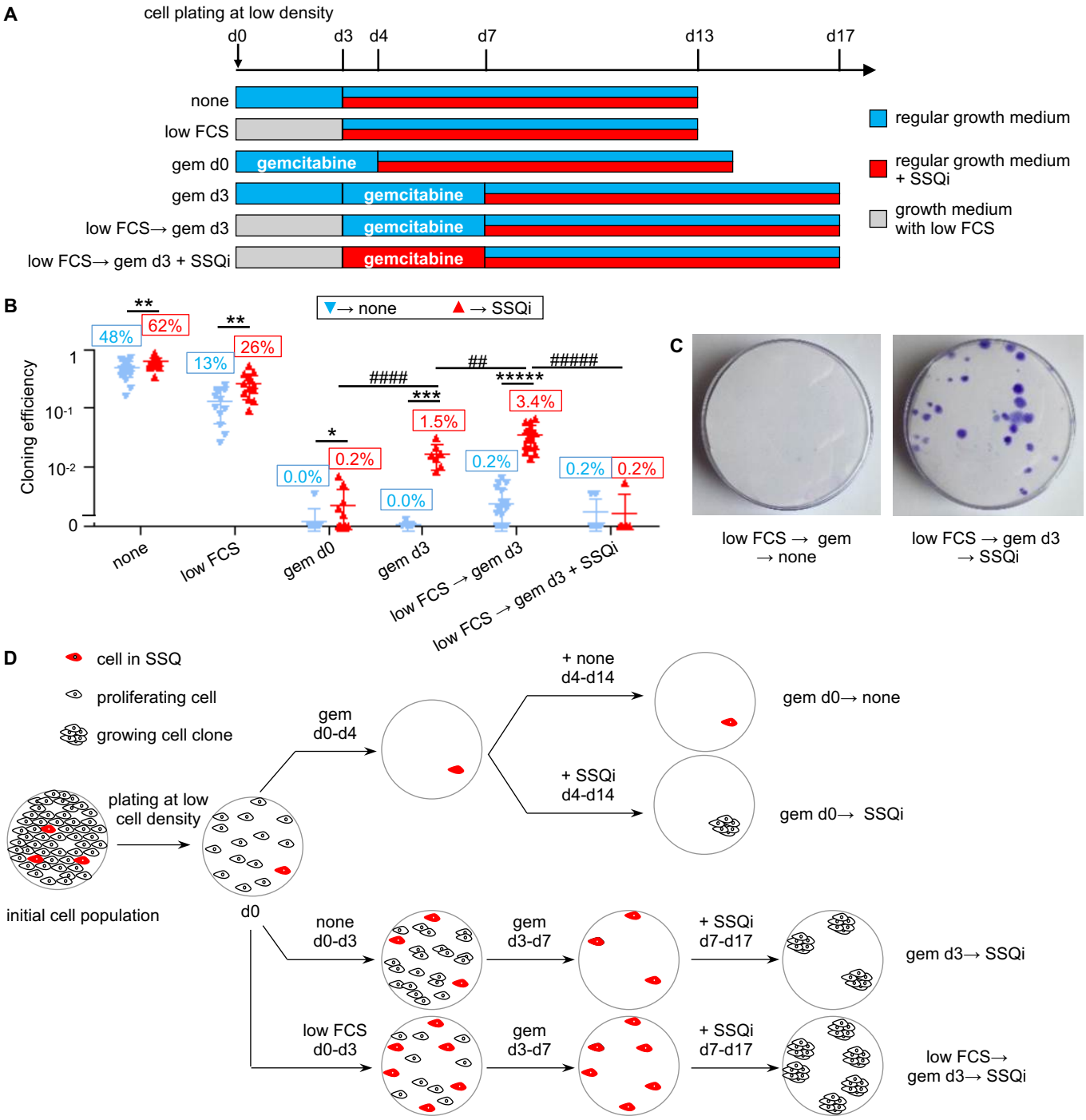
A
cell plating at low density
d0
d3
d4
d7
d13
d17
none
low FCS
gem d0
gem d3
low FCS→ gem d3
low FCS→ gem d3 + SSQi
gemcitabine
regular growth medium
regular growth medium + SSQi
growth medium with low FCS
B
▼→ none
▲ → SSQi
Cloning efficiency
48%
62%
13%
26%
0.0%
0.2%
0.0%
1.5%
0.2%
3.4%
0.2%
0.2%
none
low FCS
gem d0
gem d3
low FCS → gem d3
low FCS → gem d3 + SSQi
C
low FCS → gem → none
low FCS → gem d3 → SSQi
D
cell in SSQ
proliferating cell
growing cell clone
initial cell population
plating at low cell density
d0
gem d0-d4
+ none d4-d14
gem d0→ none
+ SSQi d4-d14
gem d0→ SSQi
none d0-d3
gem d3-d7
+ SSQi d7-d17
gem d3→ SSQi
low FCS d0-d3
gem d3-d7
+ SSQi d7-d17
low FCS→ gem d3→ SSQi

Figure 2

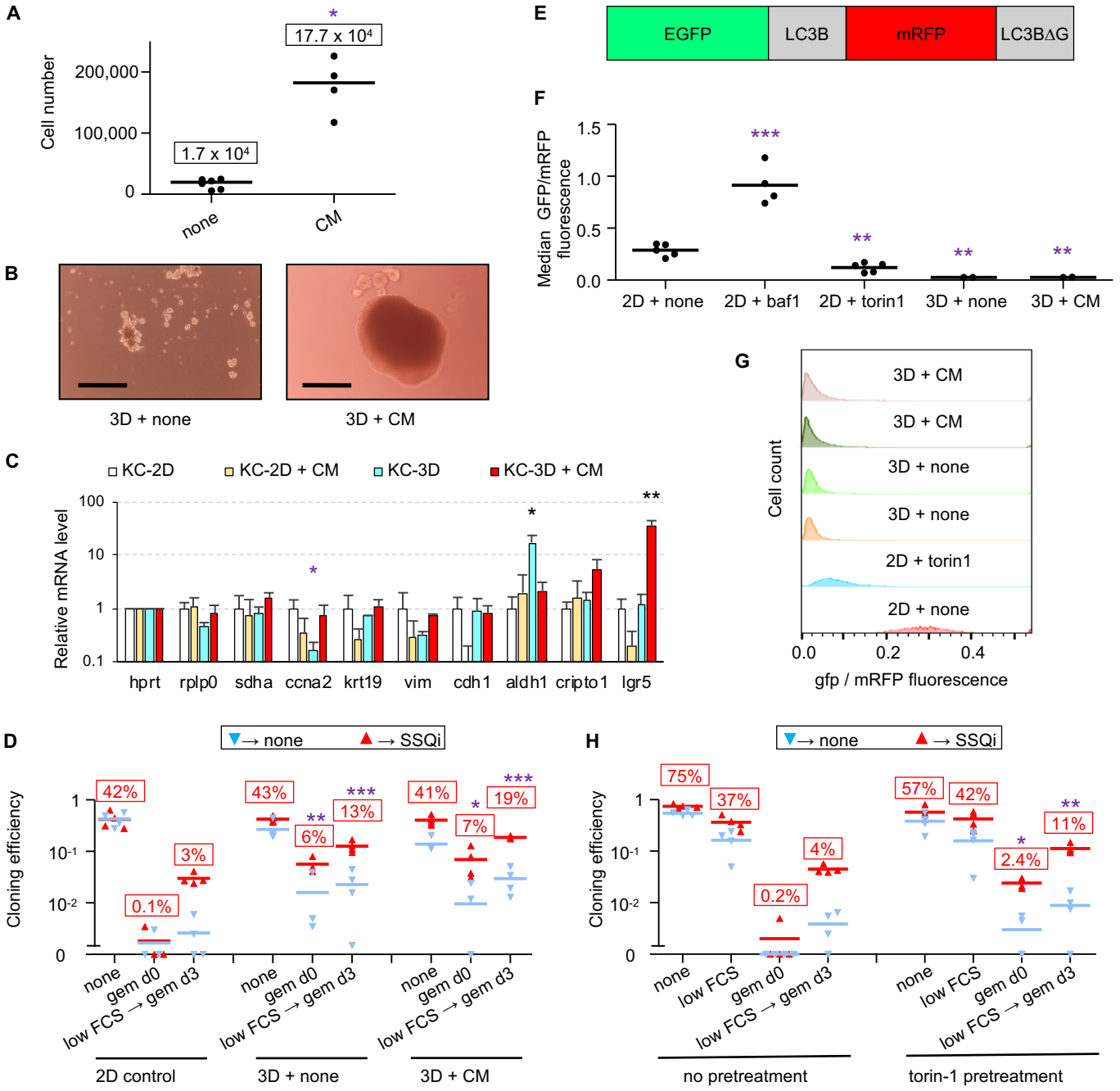
A
Cell number
200,000
100,000
0
1.7 x 10⁴
17.7 x 10⁴
*
none
CM
B
3D + none
3D + CM
C
KC-2D
KC-2D + CM
KC-3D
KC-3D + CM
Relative mRNA level
100
10
1
0.1
hprt
rplp0
sdha
ccna2
krt19
vim
cdh1
aldh1
cripto1
lgr5
D
→ none
→ SSQi
Cloning efficiency
42%
0.1%
3%
43%
6%
13%
41%
7%
19%
none
gem d0
low FCS → gem d3
2D control
3D + none
3D + CM
E
EGFP
LC3B
mRFP
LC3BΔG
F
Median GFP/mRFP fluorescence
1.5
1.0
0.5
0.0
2D + none
2D + baf1
2D + torin1
3D + none
3D + CM
G
Cell count
3D + CM
3D + CM
3D + none
3D + none
2D + torin1
2D + none
0.0
0.2
0.4
gfp / mRFP fluorescence
H
→ none
→ SSQi
Cloning efficiency
75%
37%
0.2%
4%
57%
42%
2.4%
11%
none
low FCS
gem d0
low FCS → gem d3
no pretreatment
torin-1 pretreatment

Figure 3

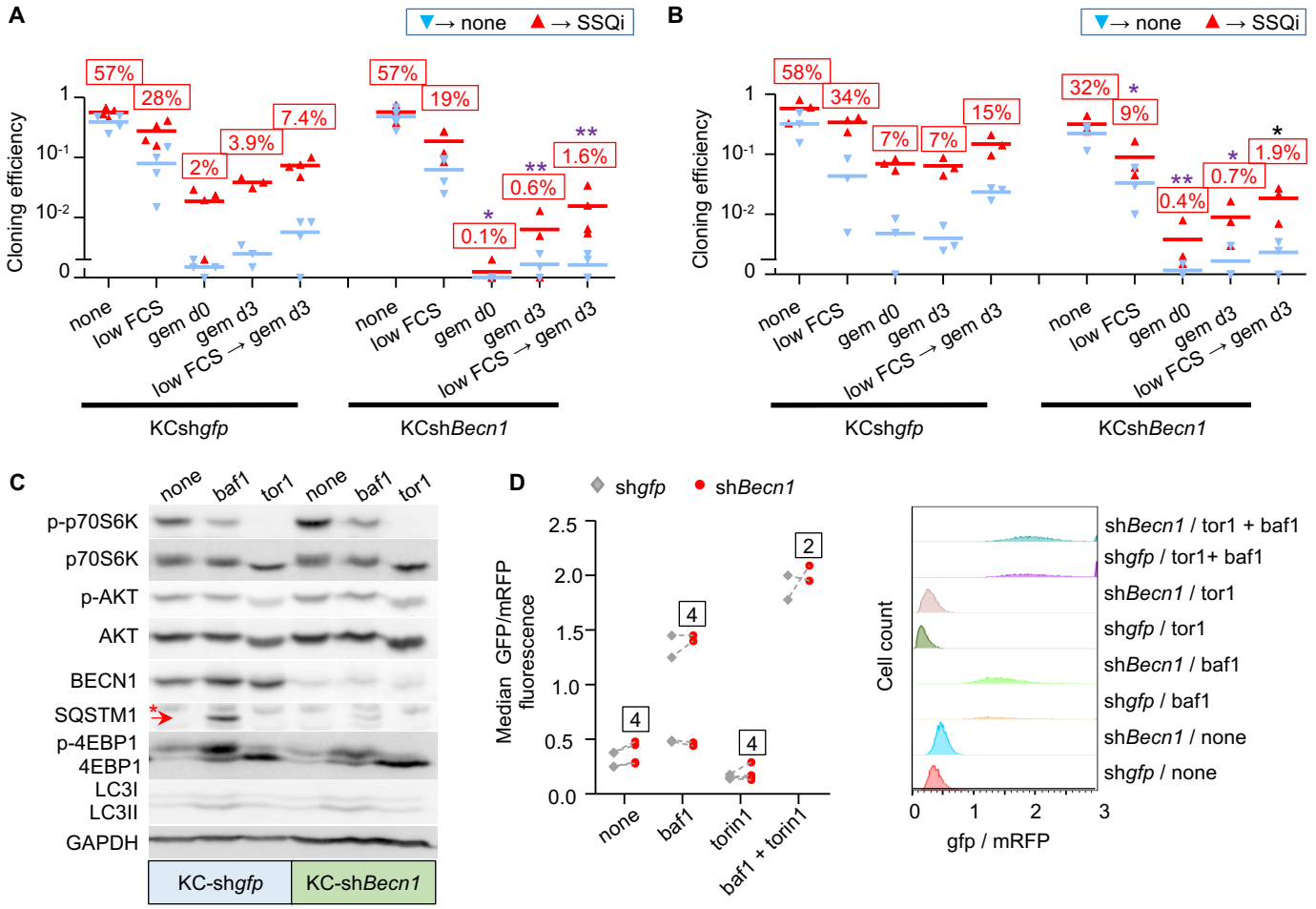
A
▼→ none ▲ → SSQi
Cloning efficiency
57%
28%
2%
3.9%
7.4%
57%
19%
0.1%
0.6%
1.6%
none
low FCS
gem d0
gem d3
low FCS → gem d3
KCshgfp
KCshBecn1
B
58%
34%
7%
7%
15%
32%
9%
0.4%
0.7%
1.9%
C
none
baf1
tor1
p-p70S6K
p70S6K
p-AKT
AKT
BECN1
SQSTM1
p-4EBP1
4EBP1
LC3I
LC3II
GAPDH
KC-shgfp
KC-shBecn1
D
shgfp
shBecn1
Median GFP/mRFP fluorescence
torin1
baf1 + torin1
Cell count
gfp / mRFP
shBecn1 / tor1 + baf1
shgfp / tor1+ baf1
shBecn1 / tor1
shgfp / tor1
shBecn1 / baf1
shgfp / baf1
shBecn1 / none
shgfp / none

Figure 4

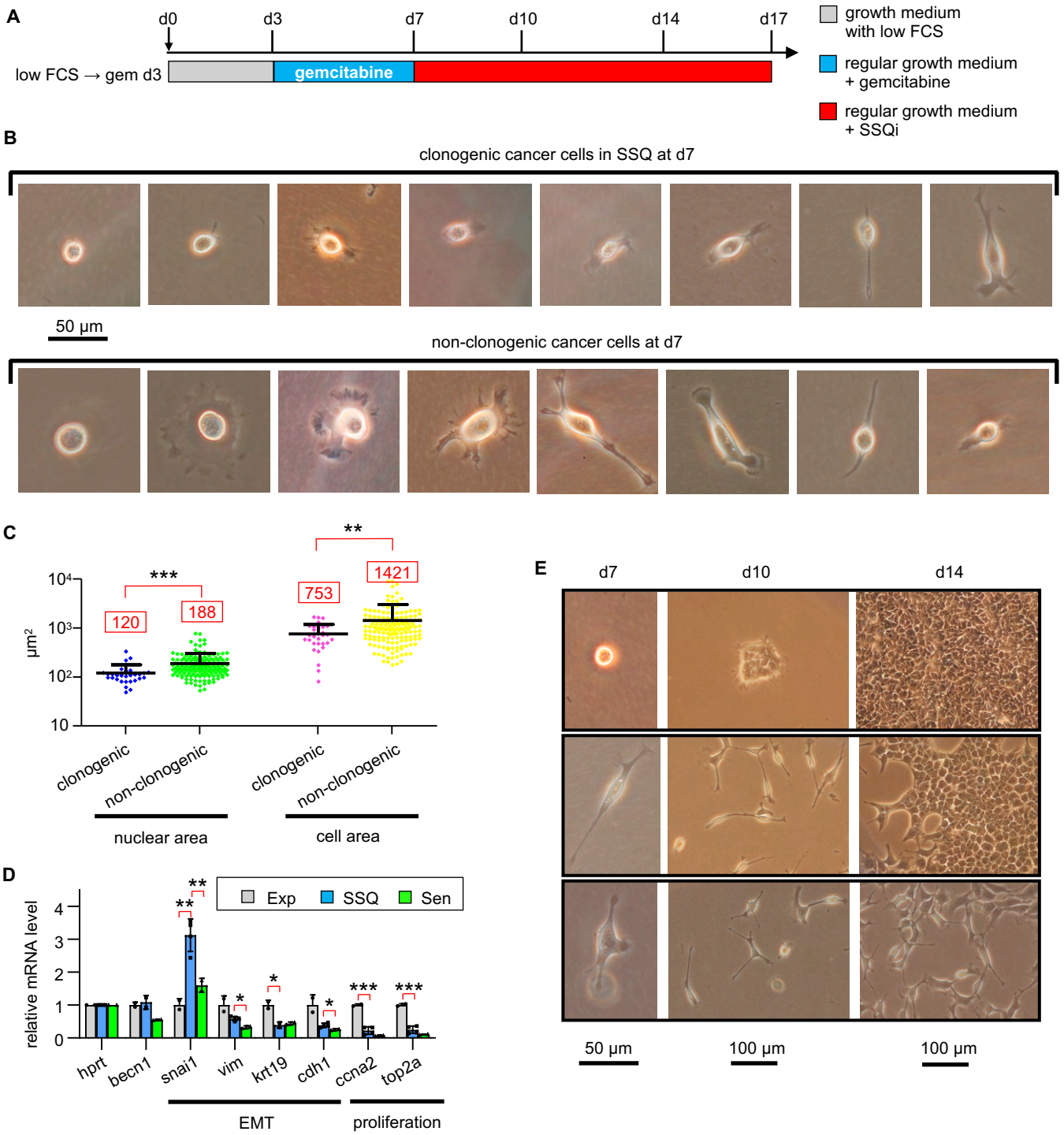
A
d0
d3
d7
d10
d14
d17
low FCS → gem d3
gemcitabine
growth medium with low FCS
regular growth medium + gemcitabine
regular growth medium + SSQi
B
clonogenic cancer cells in SSQ at d7
50 µm
non-clonogenic cancer cells at d7
C
µm²
120
188
753
1421
clonogenic
non-clonogenic
clonogenic
non-clonogenic
nuclear area
cell area
D
relative mRNA level
Exp
SSQ
Sen
hprt
becn1
snai1
vim
krt19
cdh1
ccna2
top2a
EMT
proliferation
E
d7
d10
d14
50 µm
100 µm
100 µm

Figure 5

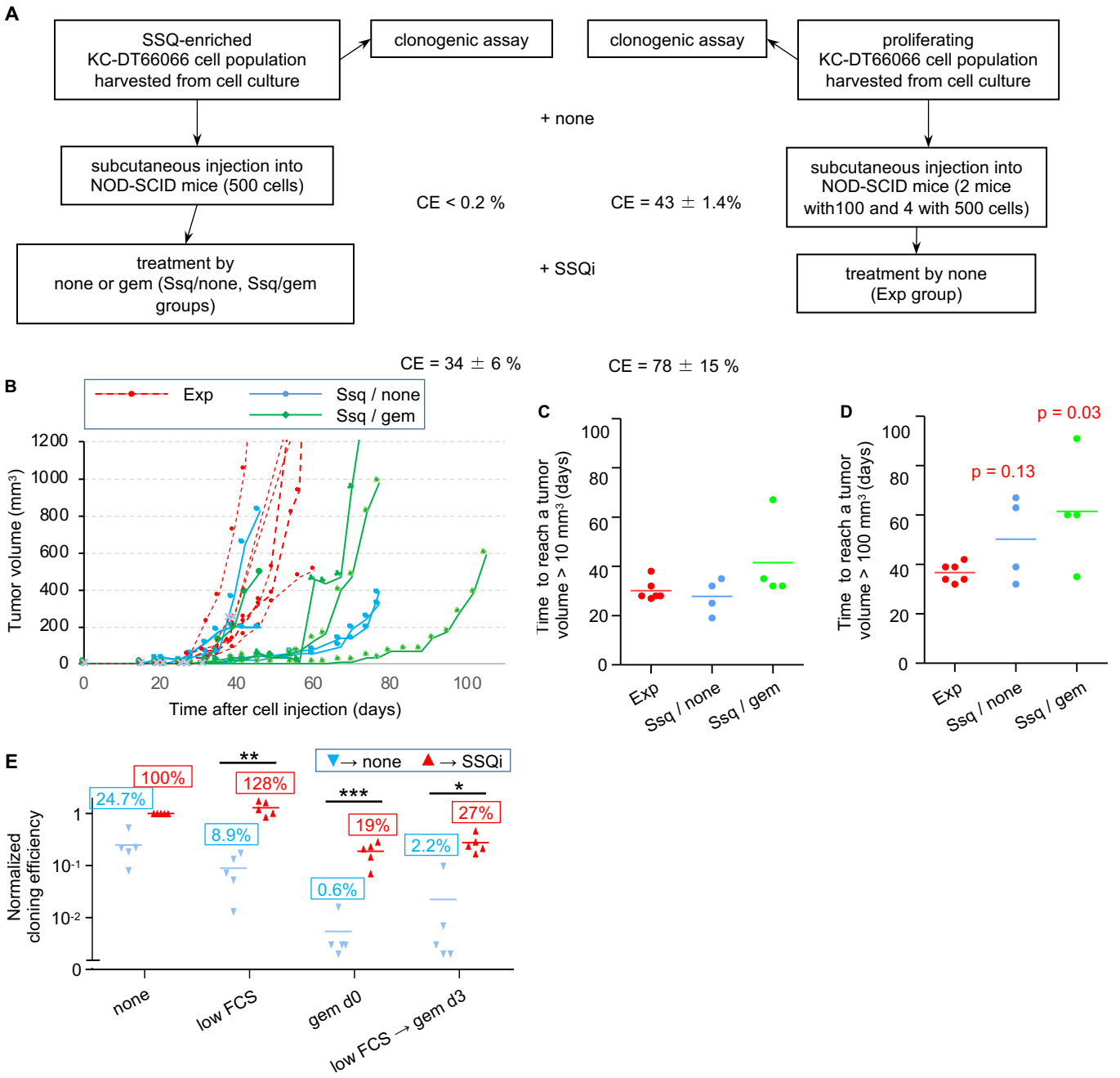
A
SSQ-enriched KC-DT66066 cell population harvested from cell culture
clonogenic assay
clonogenic assay
proliferating KC-DT66066 cell population harvested from cell culture
+ none
subcutaneous injection into NOD-SCID mice (500 cells)
CE < 0.2 %
CE = 43 ± 1.4%
subcutaneous injection into NOD-SCID mice (2 mice with100 and 4 with 500 cells)
treatment by none or gem (Ssq/none, Ssq/gem groups)
+ SSQi
treatment by none (Exp group)
CE = 34 ± 6 %
CE = 78 ± 15 %
B
Exp
Ssq / none
Ssq / gem
Tumor volume (mm³)
Time after cell injection (days)
C
Time to reach a tumor volume > 10 mm³ (days)
Exp
Ssq / none
Ssq / gem
D
p = 0.03
p = 0.13
Time to reach a tumor volume > 100 mm³ (days)
Exp
Ssq / none
Ssq / gem
E
▼→ none
▲ → SSQi
Normalized cloning efficiency
24.7%
100%
8.9%
128%
0.6%
19%
2.2%
27%
**
***
*
none
low FCS
gem d0
low FCS → gem d3

Figure 6

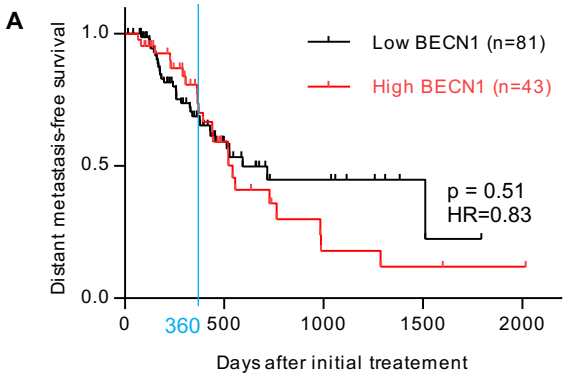
A
Distant metastasis-free survival
1.0
0.5
0.0
Low BECN1 (n=81)
High BECN1 (n=43)
p = 0.51
HR=0.83
0
360
500
1000
1500
2000
Days after initial treatement

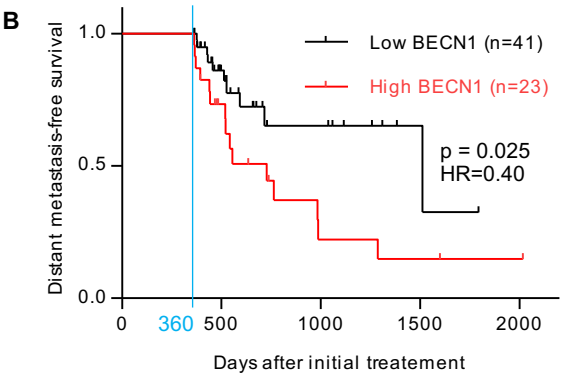
B
Distant metastasis-free survival
1.0
0.5
0.0
Low BECN1 (n=41)
High BECN1 (n=23)
p = 0.025
HR=0.40
0
360
500
1000
1500
2000
Days after initial treatement

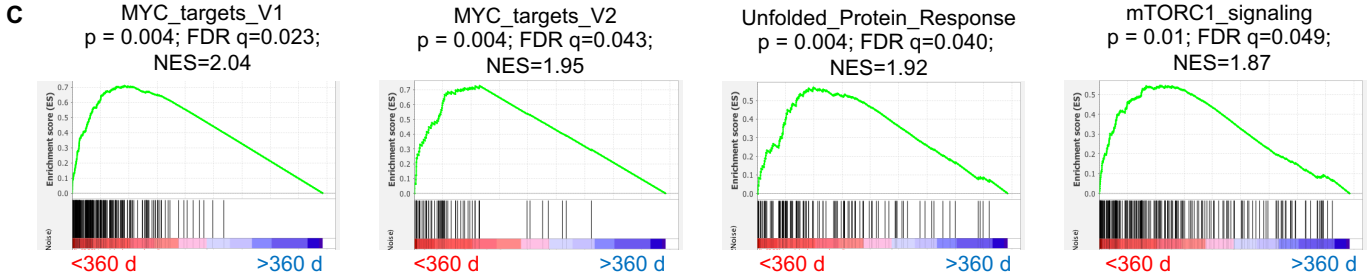
C
MYC_targets_V1
p = 0.004; FDR q=0.023;
NES=2.04
<360 d
>360 d
MYC_targets_V2
p = 0.004; FDR q=0.043;
NES=1.95
<360 d
>360 d
Unfolded_Protein_Response
p = 0.004; FDR q=0.040;
NES=1.92
<360 d
>360 d
mTORC1_signaling
p = 0.01; FDR q=0.049;
NES=1.87
<360 d
>360 d

Figure 7

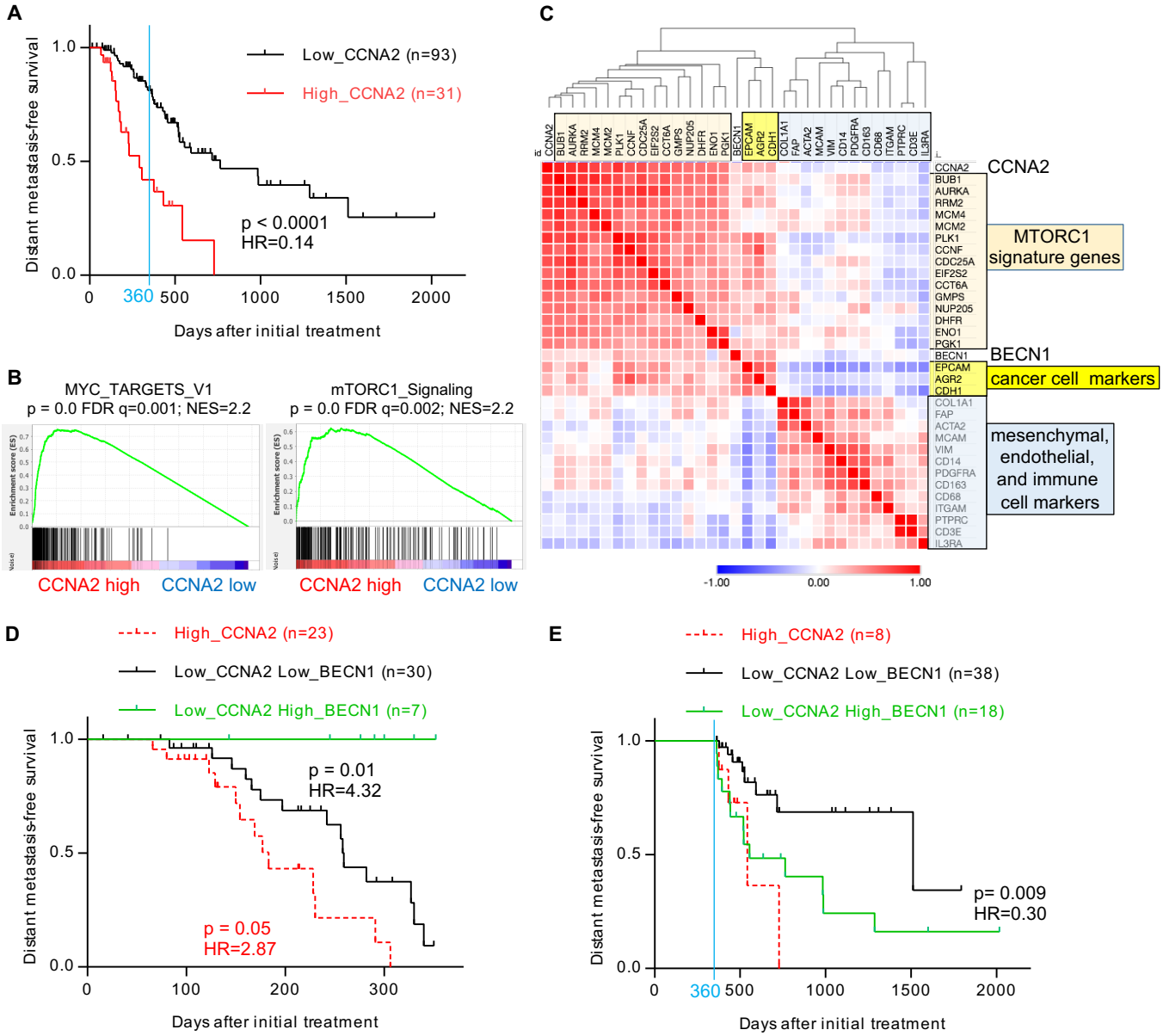
A
Distant metastasis-free survival
Low_CCNA2 (n=93)
High_CCNA2 (n=31)
p < 0.0001
HR=0.14
360
Days after initial treatment
B
MYC_TARGETS_V1
p = 0.0 FDR q=0.001; NES=2.2
mTORC1_Signaling
p = 0.0 FDR q=0.002; NES=2.2
CCNA2 high
CCNA2 low
C
CCNA2
MTORC1 signature genes
BECN1
cancer cell markers
mesenchymal, endothelial, and immune cell markers
-1.00
0.00
1.00
D
High_CCNA2 (n=23)
Low_CCNA2 Low_BECN1 (n=30)
Low_CCNA2 High_BECN1 (n=7)
p = 0.01
HR=4.32
p = 0.05
HR=2.87
Days after initial treatment
E
High_CCNA2 (n=8)
Low_CCNA2 Low_BECN1 (n=38)
Low_CCNA2 High_BECN1 (n=18)
p= 0.009
HR=0.30
Days after initial treatment

Figure 8

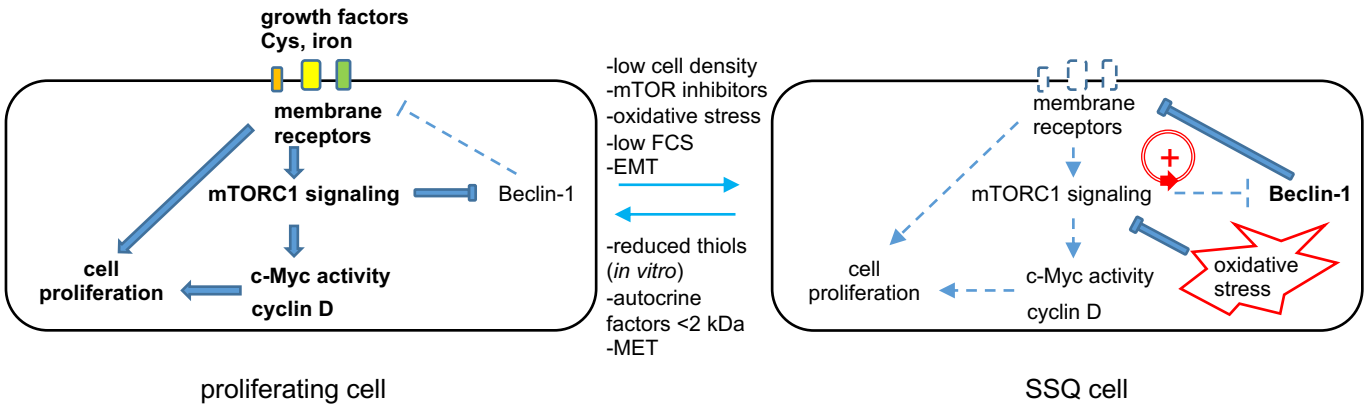
growth factors
Cys, iron
membrane
receptors
mTORC1 signaling
Beclin-1
cell
proliferation
c-Myc activity
cyclin D
-low cell density
-mTOR inhibitors
-oxidative stress
-low FCS
-EMT
-reduced thiols
(in vitro)
-autocrine
factors <2 kDa
-MET
membrane
receptors
+
mTORC1 signaling
Beclin-1
cell
proliferation
c-Myc activity
cyclin D
oxidative
stress
proliferating cell
SSQ cell